

A symbolic framework to obtain mid-fidelity models of flexible multibody systems with application to horizontal-axis wind turbines

Emmanuel Branlard¹ and Jens Geisler²

¹National Renewable Energy Laboratory, Golden, CO 80401, USA

²Hochschule Flensburg, University of Applied Sciences, 24943 Flensburg, Germany

Correspondence: E. Branlard (emmanuel.branlard@nrel.gov)

1 **Abstract.** The article presents a symbolic framework (also called computer algebra program) that is used to obtain, in symbolic
2 mathematical form, the linear and nonlinear equations of motion of a mid-fidelity multibody system including rigid and flexible
3 bodies . Our approach is based on Kane’s method and a nonlinear shape function representation for flexible bodies. The shape
4 function approach does not represent the state of the art for flexible multibody dynamics but it represents an effective trade-off to
5 obtain mid-fidelity models with few degrees of freedom and taking advantage of the separation of space and time. The method
6 yields compact symbolic equations of motion with implicit account of the constraints. The general and automatic framework
7 facilitates the creation and manipulation of models with various levels of complexity by adding or removing degrees of freedom.
8 The symbolic treatment allows for analytical gradients and linearized equations of motion. The linear and nonlinear equations
9 can be exported to Python code or dedicated software. There are multiple applications, such as time domain simulation, stability
10 analyses, frequency domain analyses, advanced controller design, state observers, and digital twins. In this article, we describe
11 the method we used to systematically generate the equations of motion of multibody systems, and present the implementation
12 of the framework using the Python package SymPy. We apply the framework to generate illustrative land-based and offshore
13 wind turbine models. We compare our results with OpenFAST simulations and discuss the advantages and limitations of the
14 method. The Python implementation is provided as an open-source project.

15 1 Introduction

16 The next generation of wind turbine digital technologies and control systems require versatile aero-servo-hydro-elastic models,
17 with various levels of fidelity, suitable for a wide range of applications. Such applications include time domain simulations, lin-
18 earization (for controller design and tuning, or frequency domain analyses), analytical gradients (for optimization procedures),
19 and generation of dedicated, high-performance or embedded code (for stand-alone simulations, state observers or digital twins).
20 Current models are implemented for a specific purpose and are usually based on an heuristic structure. Aeroelastic tools, such
21 as Flex (Øye, 1983; Branlard, 2019) or ElastoDyn (Jonkman et al., 2021), rely on an assumed chain of connections between
22 bodies, a given set of degrees of freedom, and predefined orientations of shape functions. It is not straightforward to extract
23 reduced-order models from these tools or extend the models to additional degrees of freedom.

24 Tools with linearization capabilities, such as HAWCStab2 (Sønderby and Hansen, 2014) or OpenFAST (Jonkman et al.,
25 2021) are dedicated to horizontal-axis wind turbines, and the evaluation of the gradients are limited to hard-coded analytical
26 expressions or numerical finite differences. Small implementation changes often require extensive redevelopment, and the
27 range of applications of the tools remains limited (Simani, 2015). The linear models generated by these tools are numerical
28 models that are evaluated for a given set of numerical input parameters. It is therefore difficult to obtain gradients of the
29 linear models as function of the input parameters, an information which is becoming increasingly important in optimization
30 frameworks and controls co-design approaches (Jonkman et al., 2022).

31 To address these issues, we propose a symbolic framework (also called a computer algebra program) for the automatic
32 derivation, processing, and parameterization of models with granularity in the level of fidelity. Our approach is based on
33 Kane’s method (Kane and Wang, 1965) and a nonlinear shape function representation of flexible bodies (Shabana, 2013)
34 described using a standard input data (SID) format (Wallrapp, 1994; Schwertassek and Wallrapp, 1999). The method yields
35 compact symbolic equations of motion with implicit account of the constraints. Similar approaches have been presented in the
36 literature: Kurz and Eberhard (2009), Merz (2018), Lemmer (2018), and Branlard (2019). Our framework differs in the fact
37 that all equations are processed at a symbolic level and therefore the model can be used in its nonlinear or linearized form.
38 The linear models are obtained using analytical differentiation. They can be evaluated for various set of input parameters
39 directly and therefore be used in optimization frameworks or controls co-design approaches. We implemented an open-source
40 version in Python using SymPy (SymPy, 2021), leveraging its mechanical toolbox. Alternative symbolic frameworks found in
41 the literature are usually limited to rigid bodies (Verlinden et al., 2005; Kurz and Eberhard, 2009; Gede et al., 2013; Docquier
42 et al., 2013) or are closed-source or using proprietary software (Reckdahl and Mitiguy, 1996; Kurtz et al., 2010; MotionGenesis,
43 2016; Lemmer, 2018).

44 Kane’s method and the nonlinear shape function approach presented in this article do not represent the state of the art
45 of multibody dynamics with flexible bodies. The geometrically exact beam theory (Simo, 1985; Jelenić and Crisfield, 1999;
46 Géraudin and Cardona, 2001; Bauchau, 2011) is more precise than the shape function approach because it represents the beam
47 kinematics exactly. Linearization of the geometrical exact beam theory equations is possible and also more precise than the
48 shape function approach but it leads to larger and more involved expressions. Similarly, multipurpose multibody software exists
49 (Lange et al., 2007), such as ANSYS (ANSYS, 2022), SIMPACK (SIMPACK, 2022), or MBDyn (MBDyn, 2022). These
50 more advanced approaches target different applications than those envisioned in this study: they are suitable for numerical
51 simulations, but they cannot provide symbolic mid-fidelity models in compact form.

52 In section 2, we present the formalism used to derive the equations of motion in a systematic and unified way for flexible
53 and rigid bodies. In section 3, we give an overview of how the symbolic calculation framework was implemented. Example of
54 applications relevant to wind energy are given in section 4. Discussions and conclusions follow.

55 **2 Method to obtain the equations of motion**

56 In this section, we present the formalism used to setup the equations of motion.

57 2.1 System definition and kinematics

58 We consider a system of n_b bodies, rigid or flexible, connected by a set of joints. For simplicity, we assume that no kinematic
 59 loops are present in the system, and the masses of the bodies are constant. An inertial frame is defined to express the positions,
 60 velocities, and accelerations of the bodies. We adopt a minimal set of generalized coordinates, \mathbf{q} , of dimension n_q , to describe
 61 the kinematics of the bodies: joint coordinates describing the joints displacements, and Rayleigh-Ritz coordinates for the
 62 amplitudes of the shape functions of the flexible bodies (see, e.g., Branlard (2019)). The choice of coordinates is left to the
 63 user, but it is assumed to form a minimal set. We will provide illustrative examples in section 4.

64 At a given time, the positions, orientations, velocities, and accelerations of all the points of the structure are entirely deter-
 65 mined by the knowledge of \mathbf{q} , $\dot{\mathbf{q}}$, and $\ddot{\mathbf{q}}$, where $(\dot{\quad})$ represents the time derivative. For a given body i , and a point P belonging
 66 to the body, the position, velocity, and acceleration of the point are given by (see, e.g., Shabana (2013)):

$$67 \quad \mathbf{r}_P = \mathbf{r}_i + \mathbf{s}_P = \mathbf{r}_i + \mathbf{s}_{P_0} + \mathbf{u}_P \quad (1)$$

$$68 \quad \mathbf{v}_P = \mathbf{v}_i + \boldsymbol{\omega}_i \times \mathbf{s}_P + (\dot{\mathbf{u}}_P)_i \quad (2)$$

$$69 \quad \mathbf{a}_P = \mathbf{a}_i + \boldsymbol{\omega}_i \times (\boldsymbol{\omega}_i \times \mathbf{s}_P) + \dot{\boldsymbol{\omega}}_i \times \mathbf{s}_P + 2\boldsymbol{\omega}_i \times (\dot{\mathbf{u}}_P)_i + (\ddot{\mathbf{u}}_P)_i \quad (3)$$

70 where \mathbf{r}_i , \mathbf{v}_i , and \mathbf{a}_i are the position, velocity, and acceleration of the origin of the body, respectively; \mathbf{s}_{P_0} is the initial
 71 (undeformed) position vector of point P with respect to the body origin; the subscript P is used for the deformed position
 72 of the point and P_0 for the undeformed position; \mathbf{u}_P is the elastic displacement of the point (equal to 0 for rigid bodies);
 73 $\boldsymbol{\omega}_i$ is the rotational velocity of the body with respect to the inertial frame; $(\dot{\quad})$ and $(\dot{\quad})_i$ refer to time derivatives in the inertial
 74 and body frame respectively. Throughout the article, we use bold symbols for vectors and matrices, and uppercase symbols
 75 for most matrices. The elastic displacement is obtained as a superposition of elastic deformations (see subsection 2.4). We
 76 define the transformation matrix \mathbf{R}_i that transforms coordinates from the body frame to the inertial frame, and by definition
 77 $[\tilde{\boldsymbol{\omega}}_i] = \dot{\mathbf{R}}_i \mathbf{R}_i^T$, where $[\tilde{\quad}]$ represents the skew symmetric matrix, and the exponent T denotes the matrix transpose. We assume
 78 that vectors are represented as column vectors to conveniently introduce matrix-vector multiplications. We use the notation “ \cdot ”
 79 to indicate the dot product between two vectors (irrespective of their column or row representation).

80 2.2 Introduction to Kane’s method

81 Kane’s method (Kane and Wang, 1965) is a powerful and systematic way to obtain the equations of motion of a system. The
 82 procedure leads to n_q coupled equations of motion:

$$83 \quad \mathbf{f}_r + \mathbf{f}_r^* = 0, \quad r = 1 \dots n_q \quad (4)$$

84 where \mathbf{f}_r^* is associated with inertial loads and \mathbf{f}_r is associated with external loads, and these components are obtained for all
 85 generalized coordinates. The components are obtained as a superposition of contributions from each body:

$$86 \quad \mathbf{f}_r = \sum_{i=1}^{n_b} \mathbf{f}_{ri}, \quad \mathbf{f}_r^* = \sum_{i=1}^{n_b} \mathbf{f}_{ri}^* \quad (5)$$

87 The terms \mathbf{f}_{ri} and \mathbf{f}_{ri}^* can be obtained for each body individually and assembled at the end to form the final system of equa-
 88 tions. We will present in subsection 2.3 and subsection 2.4 how these terms are defined for rigid bodies and flexible bodies,
 89 respectively.

90 2.3 Rigid bodies

91 We assume that body i is a rigid body and proceed to define the terms \mathbf{f}_{ri} and \mathbf{f}_{ri}^* . The inertial force, \mathbf{f}_i^* , and inertial torque,
 92 $\boldsymbol{\tau}_i^*$, acting on the body are:

$$93 \quad \mathbf{f}_i^* = -m_i \mathbf{a}_{G,i}, \quad \boldsymbol{\tau}_i^* = -\mathbf{I}_{G,i} \cdot \dot{\boldsymbol{\omega}}_i - \boldsymbol{\omega}_i \times (\mathbf{I}_{G,i} \cdot \boldsymbol{\omega}_i) \quad (6)$$

94 where m_i is the mass of the body, $\mathbf{a}_{G,i}$ is the acceleration of its center of mass with respect to the inertial frame, and $\mathbf{I}_{G,i}$ is the
 95 inertial tensor of the body expressed at its center of mass. Equation 6 is a vectorial relationship; it may therefore be evaluated
 96 in any coordinate system. The component \mathbf{f}_{ri}^* is defined as:

$$97 \quad \mathbf{f}_{ri}^* = \mathbf{J}_{v,ri} \cdot \mathbf{f}_i^* + \mathbf{J}_{\omega,ri} \cdot \boldsymbol{\tau}_i^* \quad (7)$$

98 with

$$99 \quad \mathbf{J}_{v,ri} = \frac{\partial \mathbf{v}_{G,i}}{\partial \dot{q}_r}, \quad \mathbf{J}_{\omega,ri} = \frac{\partial \boldsymbol{\omega}_i}{\partial \dot{q}_r} \quad (8)$$

100 where $\mathbf{v}_{G,i}$ is the velocity of the body mass center with respect to the inertial frame. The partial velocities, or Jacobians, \mathbf{J}_v
 101 and \mathbf{J}_ω , are key variables of the Kane's method. They project the physical coordinates into the generalized coordinates (\mathbf{q}),
 102 inherently accounting for the kinematic constraints between bodies. In numerical implementations, the Jacobians are typically
 103 stored in matricial forms, referred to as "velocity transformation matrices." The terms \mathbf{f}_{ri}^* can equivalently be obtained using the
 104 partial velocity of any body point (e.g., the origin) by carefully transferring the inertial loads to the chosen point. The external
 105 forces and torques acting on the body are combined into an equivalent force and torque acting at the center of mass, written as
 106 \mathbf{f}_i and $\boldsymbol{\tau}_i$. The component \mathbf{f}_{ri} is then given by:

$$107 \quad \mathbf{f}_{ri} = \mathbf{J}_{v,ri} \cdot \mathbf{f}_i + \mathbf{J}_{\omega,ri} \cdot \boldsymbol{\tau}_i \quad (9)$$

108 Equivalently, the contributions from each individual force, $\mathbf{f}_{i,j}$, acting on a point P_j of the body i , and each torque, $\boldsymbol{\tau}_{i,k}$, can
 109 be summed using the appropriate partial velocity to obtain \mathbf{f}_{ri} :

$$110 \quad \mathbf{f}_{ri} = \sum_j \frac{\partial \mathbf{v}_{P_j}}{\partial \dot{q}_r} \cdot \mathbf{f}_{i,j} + \sum_k \mathbf{J}_{\omega,ri} \cdot \boldsymbol{\tau}_{i,k} \quad (10)$$

111 where \mathbf{v}_{P_j} is the velocity of the point j with respect to the inertial frame. Equation 7 and Equation 9 are inserted into Equation 5
 112 to obtain the final equations of motion.

113 2.4 Flexible bodies

114 We assume that body i is a flexible body and proceed to define the terms f_{r_i} and $f_{r_i}^*$. The dynamics of a flexible body are
 115 described in standards textbooks such as Shabana (2013) or Schwertassek and Wallrapp (1999). Unlike rigid bodies, the equa-
 116 tions for flexible bodies are typically expressed with respect to a reference point different from the center of mass. We will call
 117 this point the origin and write it O_i . The elastic displacement field of the body is written as \mathbf{u} . It defines the displacement of any
 118 point of the body with respect to its undeformed position. Using the zeroth-order¹ Rayleigh-Ritz approximation, the displace-
 119 ment field at a given point, P , is given by the sum of shape function contributions: $\mathbf{u}(P) = \sum_{j=1}^{n_{e,i}} \Phi_{ij}(P) \mathbf{q}_{e,ij}(t)$, where Φ_{ij}
 120 are the shape functions (displacement fields) of body i , and $\mathbf{q}_{e,ij}$ is the subset of \mathbf{q} consisting of the elastic coordinates of body
 121 i , of size $n_{e,i}$. The principles of the shape function approach applied to beams are given in Appendix B. The shape functions
 122 are more easily represented in the body coordinate system. Vectors and matrices that are explicitly written in the body frame
 123 will be written with primes. The equations of motion of the flexible bodies are (Wallrapp, 1994):

$$124 \begin{bmatrix} M'_{xx} & M'_{x\theta} & M'_{xe} \\ & M'_{\theta\theta} & M'_{\theta e} \\ \text{sym.} & & M'_{ee} \end{bmatrix}_i \begin{bmatrix} \mathbf{a}'_i \\ \dot{\boldsymbol{\omega}}'_i \\ \ddot{\mathbf{q}}_{e,i} \end{bmatrix}_i + \begin{bmatrix} \mathbf{k}'_{\omega,x} \\ \mathbf{k}'_{\omega,\theta} \\ \mathbf{k}'_{\omega,e} \end{bmatrix}_i + \begin{bmatrix} 0 \\ 0 \\ \mathbf{k}_e \end{bmatrix}_i = \begin{bmatrix} \mathbf{f}'_x \\ \mathbf{f}'_\theta \\ \mathbf{f}'_e \end{bmatrix}_i \quad (11)$$

125 where the x , θ , and e , subscripts respectively indicate the translation, rotation, and elastic components; \mathbf{M} is the mass matrix
 126 of dimension $6 + n_{e,i}$ made of the block matrices $\mathbf{M}_{xx}, \dots, \mathbf{M}_{ee}$; \mathbf{a}_i and $\dot{\boldsymbol{\omega}}_i$ are the linear and angular acceleration of the body
 127 (origin) with respect to the inertial frame; \mathbf{k}_ω are the centrifugal, gyration, and Coriolis loads, also called quadratic velocity
 128 loads; \mathbf{k}_e are the elastic strain loads, which may contain geometric stiffening effects; \mathbf{f} are the external forces, torques, and
 129 elastic generalized forces. The different components of \mathbf{M} , \mathbf{k}_ω , \mathbf{k}_e , and \mathbf{f} are given in Appendix A. These terms depend on \mathbf{q} ,
 130 $\dot{\mathbf{q}}$, and Φ_i . The inertial force, torque, and elastic loads are:

$$131 \mathbf{f}_i^* = -\mathbf{R}_i [\mathbf{M}'_{xx} \mathbf{a}'_i + \mathbf{M}'_{x\theta} \dot{\boldsymbol{\omega}}'_i + \mathbf{M}'_{xe} \ddot{\mathbf{q}}_{e,i} + \mathbf{k}'_{\omega,x}] \quad (12)$$

$$132 \boldsymbol{\tau}_i^* = -\mathbf{R}_i [\mathbf{M}'_{\theta x} \mathbf{a}'_i + \mathbf{M}'_{\theta\theta} \dot{\boldsymbol{\omega}}'_i + \mathbf{M}'_{\theta e} \ddot{\mathbf{q}}_{e,i} + \mathbf{k}'_{\omega,\theta}] \quad (13)$$

$$133 \mathbf{h}_i^* = - [\mathbf{M}'_{ex} \mathbf{a}'_i + \mathbf{M}'_{e\theta} \dot{\boldsymbol{\omega}}'_i + \mathbf{M}'_{ee} \ddot{\mathbf{q}}_{e,i} + \mathbf{k}'_{\omega,e}] \quad (14)$$

134 The external and elastic loads are:

$$135 \mathbf{f}_i = \mathbf{R}_i \mathbf{f}'_x \quad (15)$$

$$136 \boldsymbol{\tau}_i = \mathbf{R}_i \mathbf{f}'_\theta \quad (16)$$

$$137 \mathbf{h}_i = \mathbf{f}'_e - \mathbf{k}_e \quad (17)$$

138 The components of $f_{r_i}^*$ and f_{r_i} , for $r = 1 \dots n_q$, are then defined as:

$$139 f_{r_i}^* = \mathbf{J}_{v,ri} \cdot \mathbf{f}'_i + \mathbf{J}_{\omega,ri} \cdot \boldsymbol{\tau}'_i + \mathbf{J}_{e,ri} \cdot \mathbf{h}'_i \quad (18)$$

$$140 f_{r_i} = \mathbf{J}_{v,ri} \cdot \mathbf{f}_i + \mathbf{J}_{\omega,ri} \cdot \boldsymbol{\tau}_i + \mathbf{J}_{e,ri} \cdot \mathbf{h}_i \quad (19)$$

¹We address the first-order approximation in Appendix D4.

141 with

$$142 \quad \mathbf{J}_{v,ri} = \frac{\partial \mathbf{v}_{O,i}}{\partial \dot{q}_r}, \quad \mathbf{J}_{\omega,ri} = \frac{\partial \boldsymbol{\omega}_i}{\partial \dot{q}_r}, \quad \mathbf{J}_{e,ri} = \frac{\partial \mathbf{q}_{e,i}}{\partial q_r} \quad (20)$$

143 where $\mathbf{v}_{O,i}$ is the velocity of the body with respect to the inertial frame. The term $\mathbf{J}_{e,ri}$ consists of 0 and 1 because $\mathbf{q}_{e,i}$ is a
 144 subset of \mathbf{q} . Equation 18 and Equation 19, once evaluated for body i , are inserted into Equation 5 to obtain the final equations
 145 of motion.

146 2.5 Nonlinear and linear equations of motion

147 The n_q equations of motion given in Equation 4 are gathered into a vertical vector \mathbf{e} . They are recast into the form:

$$148 \quad \mathbf{e}(\mathbf{q}, \dot{\mathbf{q}}, \ddot{\mathbf{q}}, \mathbf{u}, t) = \mathbf{f} + \mathbf{f}^* = \mathbf{F}(\mathbf{q}, \dot{\mathbf{q}}, \mathbf{u}, t) - \mathbf{M}(\mathbf{q})\ddot{\mathbf{q}} = \mathbf{0} \quad (21)$$

149 or

$$150 \quad \mathbf{M}(\mathbf{q})\ddot{\mathbf{q}} = \mathbf{F}(\mathbf{q}, \dot{\mathbf{q}}, \mathbf{u}, t) \quad (22)$$

151 where $\mathbf{M} = -\frac{\partial \mathbf{e}}{\partial \ddot{\mathbf{q}}}$ is the system mass matrix and \mathbf{F} is the forcing term vector—that is, the remainder terms of the equation
 152 ($\mathbf{F} = \mathbf{e} + \mathbf{M}\ddot{\mathbf{q}}$). The vector \mathbf{u} is introduced to represent the time-dependent inputs that are involved in the determination of the
 153 external loads. Both sides of the equations are also dependent on some parameters, but this dependency is omitted to shorten
 154 notations. The stiffness and damping matrices may be obtained by computing the Jacobian of the equations of motion with
 155 respect to \mathbf{q} and $\dot{\mathbf{q}}$, respectively. The nonlinear equation given in Equation 22 is easily integrated numerically, for instance by
 156 recasting the system into a first-order system, or by using a dedicated second-order system time integrator.

157 In various applications, a linear time invariant approximation of the system is desired. Such approximation is obtained at an
 158 operating point, noted with the subscript 0, which is a solution of the nonlinear equations of motion, namely:

$$159 \quad \mathbf{e}(\mathbf{q}_0, \dot{\mathbf{q}}_0, \ddot{\mathbf{q}}_0, \mathbf{u}_0, t) = \mathbf{0} \quad (23)$$

160 The linearized equations about this operating point are obtained using a Taylor series expansion:

$$161 \quad \mathbf{M}_0(\mathbf{q}_0)\delta\ddot{\mathbf{q}} + \mathbf{C}_0(\mathbf{q}_0, \dot{\mathbf{q}}_0, \mathbf{u}_0)\delta\dot{\mathbf{q}} + \mathbf{K}_0(\mathbf{q}_0, \dot{\mathbf{q}}_0, \ddot{\mathbf{q}}_0, \mathbf{u}_0)\delta\mathbf{q} = \mathbf{Q}_0(\mathbf{q}_0, \dot{\mathbf{q}}_0, \mathbf{u}_0)\delta\mathbf{u} \quad (24)$$

162 with

$$163 \quad \mathbf{M}_0 = -\left. \frac{\partial \mathbf{e}}{\partial \ddot{\mathbf{q}}} \right|_0, \quad \mathbf{C}_0 = -\left. \frac{\partial \mathbf{e}}{\partial \dot{\mathbf{q}}} \right|_0, \quad \mathbf{K}_0 = -\left. \frac{\partial \mathbf{e}}{\partial \mathbf{q}} \right|_0, \quad \mathbf{Q}_0 = \left. \frac{\partial \mathbf{e}}{\partial \mathbf{u}} \right|_0 \quad (25)$$

164 where \mathbf{M}_0 , \mathbf{C}_0 , and \mathbf{K}_0 are the linear mass, damping, and stiffness matrices, respectively; $\mathbf{Q}_0\delta\mathbf{u}$ is the linear forcing vector
 165 (\mathbf{Q}_0 is the input matrix); δ indicates a small perturbation of the quantities; and $|_0$ indicates that the expressions are evaluated at
 166 the operating point. In practical applications, linearization is done at an operating point where the acceleration is zero ($\ddot{\mathbf{q}}_0 = 0$)
 167 and most velocities are also zero. Examples of applications of the linear equations of motion are controller design, frequency
 168 domain analyses, and stability analyses. The symbolic system matrices also allow for the easy formulation of linear parameter-
 169 varying models used in many advanced control applications.

170 3 Implementation into a symbolic framework

171 In this section, we discuss the Python open-source symbolic calculation framework that we implemented according to the
172 equations given in section 2. A Maxima implementation from the same authors is also available (Geisler, 2021).

173 The Python library YAMS (Yet Another Multibody Solver) started as a numerical tool published in previous work (Bran-
174 lard, 2019). The library is now supplemented with a symbolic module so that both numerical and symbolic calculations can
175 be achieved. The new implementation uses the Python symbolic calculation package SymPy (SymPy, 2021). We leveraged the
176 features present in the subpackage “mechanics,” which contains all the tools necessary to compute kinematics: the definition
177 of frames and points and the determination of positions, velocities, and accelerations. The subpackage also contains an imple-
178 mentation of Kane’s equations for rigid bodies (i.e., subsection 2.3). We were also inspired by the package PyDy (Gede et al.,
179 2013), which is a convenient tool to export the equations of motion to executable code and directly visualize the bodies in 3D.
180 The core of our work consisted of implementing a class to define flexible bodies (`FlexibleBody`) and the corresponding
181 Kane’s method for this class (subsection 2.4).

182 For the `FlexibleBody` class, we followed the formalism of Wallrapp (1994) and implemented Taylor expansions for all
183 the terms defined in Appendix A, allowing the symbolic computation with Taylor expansions to any order. In practice, a zeroth-
184 or first-order expansion is used. The use of Taylor expansions is presented in Appendix D3. The different Taylor coefficients
185 may be kept as symbolic terms, or replaced early on by numerical values provided by a SID, for instance.

186 We structured the code into three layers: 1) The low-level layer integrates seamlessly with SymPy and PyDy by using the
187 `FlexibleBody` class we provide. It is the layer that offers the highest level of granularity and control for the user, since
188 arbitrary systems with various kinematic constraints can be implemented, at the cost of requiring more expertise. 2) The
189 second-level automates the calculation of the kinematics by introducing simple connections between rigid and flexible bodies.
190 The connections may be rigid, with constant offsets and rotations, or dynamic. A connection from a flexible body to another
191 body is assumed to occur at one extremity of the flexible body. Some knowledge of SymPy mechanics is still required to use
192 this layer. 3) The third level consists of template models such as generic land-based or offshore wind turbine models. Degrees
193 of freedom are easily turned on and off for these conceptual models depending on the level of fidelity asked by the user, and
194 generic external forces can be implemented or declared as external inputs.

195 The overall workflow for typical usage of the symbolic framework is illustrated in Figure 1. The symbolic framework takes
196 as input a conceptual model of the structure, which is assembled using one of the three layers previously described. The
197 nonlinear and linear equations of motion can be exported to LaTeX and Python-ready scripts for various applications (see
198 subsection 5.1). Using the third layer, as little as three lines of code are required by the user to perform the full step from
199 derivation of the equations, optional linearization, and exportation. To obtain numerical results from the exported Python code,
200 the user needs to provide the arrays with the degrees of freedom values \mathbf{q} and $\dot{\mathbf{q}}$, their initial conditions, a dictionary with
201 inputs (\mathbf{u}) that are functions of time, and a dictionary of parameters (\mathbf{p}) containing all the numerical constants such as mass,
202 acceleration of gravity, and geometric parameters. We implemented various preprocessing tools in YAMS to facilitate the
203 calculation of numerical parameters, typically from a set of OpenFAST input files or by using structural parameters defined

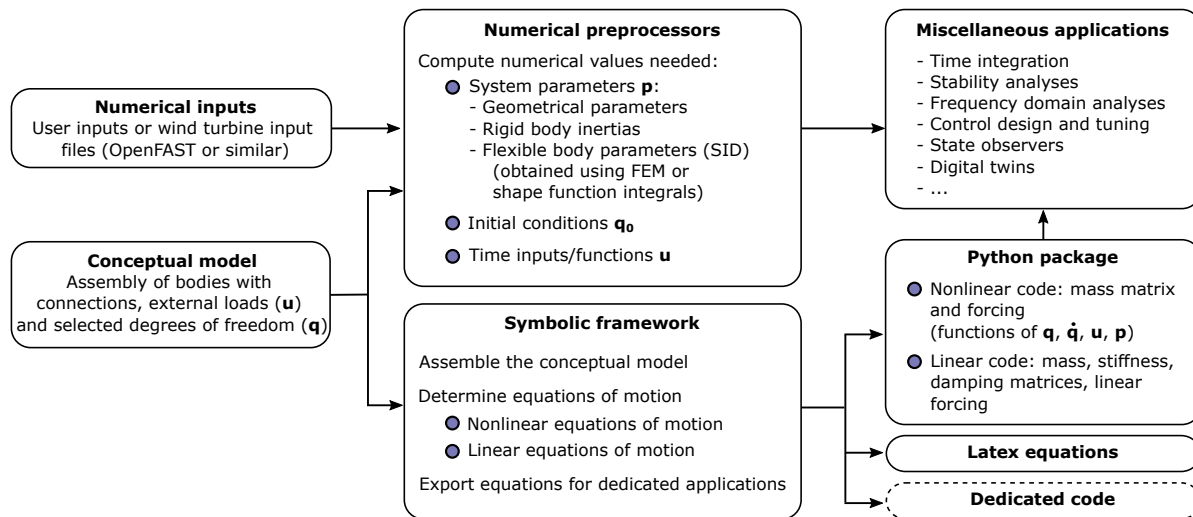


Figure 1. Typical workflow for the usage of the symbolic framework, going from numerical inputs and a conceptual model to numerical packages that can be used for various applications.

204 by the users. YAMS contains tools to compute the flexible bodies parameters (mass matrix, stiffness matrix, shape integrals)
 205 using integrals over the shape functions or using a finite-element beam formulation. YAMS also contains tools to compute the
 206 rigid body inertia of different components of a wind turbine or the full system. Postprocessing tools are also included to readily
 207 time-integrate the generated model using numerical values (including initial values).

208 The source code of YAMS is available on GitHub as a subpackage of the Wind Energy LIBrary, WELIB (Branlard, 2021).
 209 The repository contains tests and working examples, including the ones presented in section 4.

210 4 Wind energy applications

211 4.1 Approach

212 In this section, we present different wind energy applications of the symbolic framework. We focus on models with at least
 213 one flexible body because the rigid body formulation of SymPy has been well verified (Gede et al., 2013). For each example,
 214 the equations of motion are given and their results are compared with OpenFAST (Jonkman et al., 2021) simulations. This
 215 is readily achieved because our framework can export the equations of motion to Python functions, load input files from an
 216 OpenFAST model, and integrate the generated equations using the same conditions as defined in the OpenFAST input files.
 217 In this article, we do not focus on the modeling of the external loads, but we include them in the equations of motion. It is
 218 the responsibility of the user to define these functions, for instance through aero- or hydro-force models. For the verification
 219 results presented in this section, we only include the gravitational and inertial loading. In all examples, the National Renewable

220 Energy Laboratory (NREL) 5-MW reference wind turbine (Jonkman et al., 2009) is used. The examples below are provided
 221 on the GitHub repository where the YAMS package is provided (Branlard, 2021).

222 4.2 Notations

223 We adopt a system of notations where the first letter of a body is used to identify the parameters of that body. As an example,
 224 the tower is represented with the letter T, and the following body parameters are defined: T , origin; M_T , mass; L_T , length;
 225 $(J_{x,T}, J_{y,T}, J_{z,T})$, diagonal coefficients of the inertia tensor about the center of gravity and in body coordinates; \mathbf{r}_{TG} , vector
 226 from body origin to body center of mass, of coordinates (x_{TG}, y_{TG}, z_{TG}) in body coordinates. We also define θ_t , the nacelle
 227 tilt angle about the y axis; g , the acceleration of gravity along $-z$; and O , the origin of the global coordinate system.

228 4.3 Rotating blade with centrifugal stiffening

229 We begin with the study of a flexible blade of length $L_B = R$, rotating at the constant rotational speed Ω . We use this test
 230 case to familiarize the reader with the key concepts of the shape function approach given in Appendix B. A sketch of the
 231 system is given in Figure 2. We start by modeling the blade using a single shape function, assumed to be directed along the
 x -axis (“flapwise”): $\Phi_1 = \Phi e_x$, where e_x is the unit vector in the x direction. The undeflected blade is directed along the radial

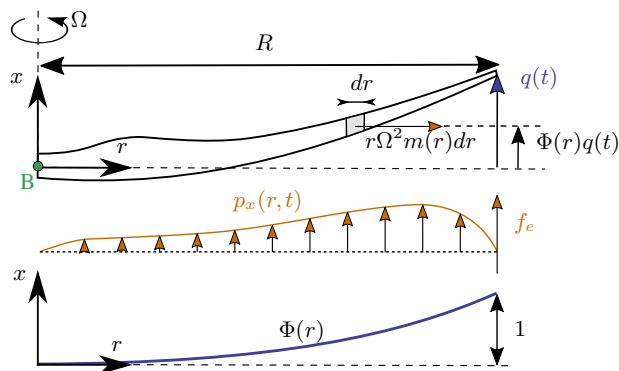


Figure 2. Sketch of a rotating blade with the restoring centrifugal force. Points are indicated in green, degrees of freedom in blue, and loads in orange.

232
 233 coordinate r and rotates around the x -axis. We assume that the shape function is known, noted $\Phi(r)$. It can be computed as the
 234 first flapwise mode of the blade using tools provided in YAMS. The expression $\Phi(r) = r^3$ is a simple approximation that can
 235 be used for hand calculations. The aerodynamic force per length in the flapwise direction is noted $p_x(r)$. The generalized mass
 236 and stiffness are computed based on the mass per length (m) and flapwise bending stiffness (EI_y) of the blade, according to

237 Equation B1:

$$238 \quad M_e = \int_0^R m(r) \Phi^2(r) dr \quad (26)$$

$$239 \quad K_e = \int_0^R EI_y(r) \left[\frac{d^2 \Phi}{dr^2}(r) \right]^2 dr \quad (27)$$

240 The generalized force is obtained from Equation B3:

$$241 \quad f_e = \int_0^R p_x(r, t) \Phi(r) dr \quad (28)$$

242 The important consideration for this model is the axial load, N . The main axial load at a radial station r comes from the
243 centrifugal force acting on all the points outboard of the current station:

$$244 \quad N(r) = \int_r^R m(r') \Omega^2 r' dr' \quad (29)$$

245 The geometric stiffness contribution of the axial load is obtained from Equation B5 as:

$$246 \quad K_g(\Omega) = \int_0^R N(r) \left[\frac{d\Phi}{dr} \right]^2 dr = \Omega^2 \int_0^R \int_r^R m(r') r' dr' \left[\frac{d\Phi}{dr} \right]^2 dr \quad (30)$$

247 The geometric stiffness, K_g , is positive and increases with the square of the rotational speed. This restoring effect is referred to
248 as “centrifugal stiffening.” In this example, the beam rotates with respect to a fixed support, the influence of gravity is omitted,
249 and no force other than the centrifugal force is assumed in the radial direction (the Coriolis force contribution to the radial
250 force is assumed to be negligible for simplicity). Therefore, the only geometric stiffness comes from the centrifugal force.
251 For a wind turbine blade mounted on a flexible support and under the influence of gravity, the different geometric stiffening
252 terms presented in Appendix C should be used. Adding the elastic and geometric stiffness, the natural frequency of the blade
253 increases with the rotational speed as follows:

$$254 \quad \omega_0(\Omega) = \sqrt{\frac{(K_e + K_g(\Omega))}{M_e}} = \sqrt{\omega_0^2(0) + \frac{K_g(\Omega)}{M_e}} = \sqrt{\omega_0^2(0) + k_\Omega \Omega^2} \quad (31)$$

255 where k_Ω is referred to as the “rise factor” or “Southwell coefficient,” and in our approximation, it is found to be constant:
256 $k_\Omega = K_g(\Omega)/M_e/\Omega^2$. The coefficient provides the variation of the blade frequency with rotational speed, which is something
257 that is observed on a Campbell diagram when performing stability analyses. In general, the mode shapes of the blade will also
258 change as a function of the rotational speed, and different shape functions should preferably be used for simulations at different
259 rotational speeds. The effect is fairly limited, and most OpenFAST practitioners only use one shape function corresponding to
260 the value at rated rotational speed. Similarly, the Southwell coefficient is a function of the rotational speed, but the variation is

261 negligible as long as the rotational speed is small compared to the natural frequency (e.g., $(\Omega/\omega)^2 \lesssim 5$; see Bielawa (2006)),
 262 which is the case for wind energy applications.

263 The treatment for a shape function in the edgewise direction is similar, using $\Phi_2 = \Phi_2 e_\theta$, where e_θ is the unit vector
 264 in the edgewise direction. In this case, the centrifugal force also has a component in the tangential direction, $p_{\theta,\text{centri}}(r) =$
 265 $-\Omega^2 u_\theta(r) dm(r)$, with $u_\theta = \Phi_2 q$. This leads to a generalized force equal to $\int_0^L p_{\theta,\text{centri}} \Phi_2 dr = -\Omega^2 M_e q$, or, equivalently, to a
 266 stiffness term: $K_\omega = -\Omega^2 M_e$. It can be verified that this generalized force corresponds to the contribution $O_{e,11} \omega_x^2$, from $\mathbf{k}_{\omega,e}$,
 267 given in Equation A10. For an edgewise mode, the frequency therefore evolves as:

$$268 \quad \omega_0(\Omega) = \sqrt{\frac{(K_e + K_g(\Omega) + K_\omega(\Omega))}{M_e}} = \sqrt{\omega_0^2(0) + (k_\Omega - 1)\Omega^2} \quad (32)$$

269 with $k_\Omega = K_g(\Omega)/M_e/\Omega^2$ and with K_g computed using Equation 30.

270 We apply the method to the NREL 5-MW wind turbine using the blade properties and shape functions provided in the Elas-
 271 toDyn input file. We order the degrees of freedom as 1st flap, 1st edge, and 2nd flap, assuming no coupling between the shape
 272 functions, so that each can be treated individually using the results from this section. The diagonal coefficients of the mass ma-
 273 trix are $\text{diag}(\mathbf{M}_e) = [9.5e3, 1.5e4, 5.7e3]$, and for the stiffness matrix they are $\text{diag}(\mathbf{K}_e) = [1.7e4, 6.7e4, 8.7e4]$, computed
 274 according to Equations 26 and 27. The coefficients k_Ω of each degree of freedom are obtained as $\mathbf{k}_\Omega = [1.7, 1.4, 5.5]$. We
 275 compare the frequencies obtained with the present method against OpenFAST linearization results in Figure 3. The simulations
 were run in vacuum (no gravity, no aerodynamics) and with a cone angle of 0 deg. Strong agreement is found for the evolution

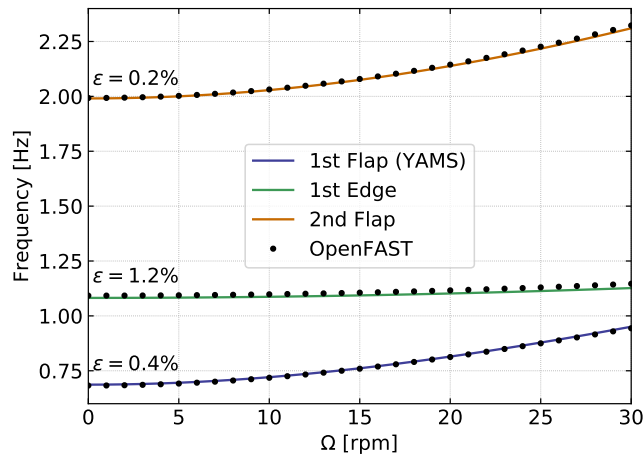


Figure 3. Variation of the natural frequencies of the NREL 5-MW turbine blade with rotational speed. Results from YAMS and OpenFAST, with mean relative error, ϵ , are reported on the figure.

276
 277 of the different frequencies with the rotational speed. The stiffening is less pronounced for edgewise modes as a result of the
 278 softening introduced by K_ω .

279 This section focused on the analysis of individual shape functions. In the general case, multiple shape functions are present
 280 and couplings might exist between them (due to the structural twist or nonorthogonality of the shape functions, or if the shape

281 functions have components in multiple directions such as $\Phi_1 = \Phi_{1x}e_x + \Phi_{1y}e_y$). In such a case, the general developments of
 282 Appendix A and Appendix B should be used.

283 4.4 Two degrees of freedom model of a land-based or fixed-bottom turbine

284 We consider a system of three bodies: tower (or support structure), nacelle, and rotor. The system represents a land-based
 wind turbine or a fixed-bottom offshore wind turbine. A sketch of the system is given in Figure 4. The nacelle and rotor

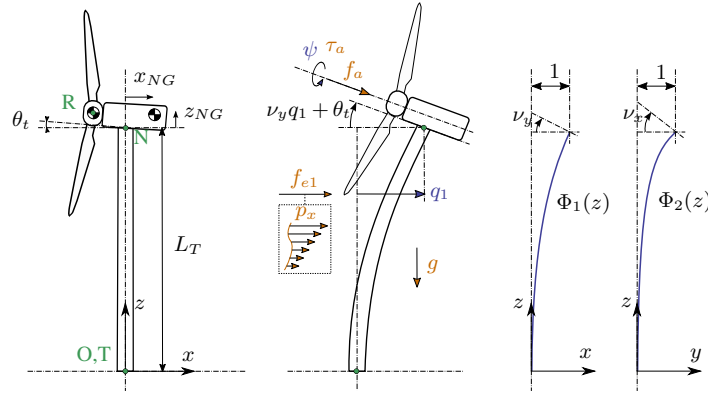


Figure 4. Model of a land-based or fixed-bottom wind turbine using one to three degrees of freedom (fore-aft and side-side flexibility of the support structure, and shaft rotation). Points are indicated in green, degrees of freedom in blue, and loads in orange.

285

286 blades are rigid bodies, whereas the tower is flexible and represented by one shape function² in the fore-aft direction, noted
 287 $\Phi_1 = \Phi_{1x}e_x$. For hand calculations and as a first approximation, the first mode shape of a massless beam with a top mass
 288 may be used: $\Phi_1(z) = 1 - \cos(z\pi/L/2)$. Increased accuracy is obtained when the shape function matches the actual first
 289 tower fore-aft bending mode, accounting for the effect of the rotor-nacelle mass and inertia. The degrees of freedom are
 290 $q = (q, \psi)$, where q is the generalized (elastic) coordinates in the fore-aft direction and ψ is the azimuthal position. The
 291 slope of the tower shape function at the tower top is a key coupling parameter of the model, noted ν_y . When the tower
 292 deflects 1 m in the x direction, the nacelle rotates by an angle ν_y . The method assumes that the tower-top point remains
 293 along the x -axis, neglecting the so-called nonlinear geometric effect. However, nonlinear geometric effects can be included
 294 using geometric stiffening corrections (see Appendix C or Branlard (2019)). The aerodynamic thrust and torque are noted
 295 f_a and τ_a , respectively, and act at the rotor center (point R). The low-speed shaft generator torque is written as τ_g . The
 296 distributed loads on the tower, p_x (from aerodynamics and hydrodynamics), are projected against the shape function to obtain
 297 the generalized forces $f_e = \int_0^{L_T} p_x(z, t)\Phi_1(z)dz$. The moments of inertia of the rotor in its coordinates are $(J_{x,R}, J_{\oplus,R}, J_{\ominus,R})$.
 298 We note that M_e, K_e , and D_e are the generalized mass, stiffness, and damping, respectively, associated with a given shape
 299 function $M_e = \int_0^{L_T} m(z)\Phi_1^2(z)dz$, $K_e = \int_0^{L_T} EI(z) \left[\frac{d^2\Phi_1(z)}{dz^2} \right]^2 dz$, $D_e = 2\zeta M_e \omega_e$. where $m(z)$ and $EI(z)$ are the mass
 300 per length and bending stiffness of the tower, respectively, and ω_e and ζ are the frequency and damping ratio, respectively,

²The relevant equations of the shape function approach for a beam are given in Appendix B.

301 associated with the shape function (assuming the shape function approximates a mode shape). The geometric softening of the
 302 tower due to the tower-top mass (K_{gt}) and its own weight (K_{gw}) is obtained using Equation B5, as $K_g = K_{gt} + K_{gw}$, with :

$$303 \quad K_{gt} = -g \int_0^{L_T} (M_R + M_N) \left[\frac{d\Phi_1}{dz}(z) \right]^2 dz \quad (33)$$

$$304 \quad K_{gw} = -g \int_0^{L_T} \left[\frac{d\Phi_1}{dz}(z) \right]^2 \left[\int_z^{L_T} m(z') dz' \right] dz \quad (34)$$

305 The tower is assumed to be fixed and under no significant vertical external loads and therefore the only geometric stiffness
 306 comes from the gravitational force. For a tower mounted on a moving support (fixed-bottom foundation or floater), additional
 307 geometric stiffening terms would be present (see Appendix C). The shape function frequency is obtained as:

$$308 \quad \omega_e = \sqrt{(K_e + K_g)/M_e} \quad (35)$$

309 The application of the symbolic framework leads to the following equations of motion (rearranged for interpretability):

$$310 \quad \begin{bmatrix} M_q & 0 \\ 0 & J_{x,R} \end{bmatrix} \begin{bmatrix} \ddot{q} \\ \ddot{\psi} \end{bmatrix} = \begin{bmatrix} f_q \\ \tau_a - \tau_g \end{bmatrix} \quad (36)$$

311 where:

$$312 \quad M_q = M_e + M_N + M_R \quad (37)$$

$$313 \quad + (J_{yN} + J_{\oplus,R} + M_N(x_{NG}^2 + z_{NG}^2) + M_R(x_{NR}^2 + z_{NR}^2))\nu_y^2 \quad (38)$$

$$314 \quad + 2[(M_N z_{NG} + M_R z_{NR}) \cos(\nu_y q) - (M_N x_{NG} + M_R x_{NR}) \sin(\nu_y q)] \nu_y \quad (39)$$

315 and

$$316 \quad f_q = f_e - (K_e + K_g)q - D_e \dot{q} \quad (40)$$

$$317 \quad + g\nu_y [(M_N x_{NG} + M_R x_{NR}) \cos(\nu_y q) + (M_N z_{NG} + M_R z_{NR}) \sin(\nu_y q)] \quad (41)$$

$$318 \quad + \nu_y^2 \dot{q}^2 [(M_N x_{NG} + M_R x_{NR}) \cos(\nu_y q) + (M_N z_{NG} + M_R z_{NR}) \sin(\nu_y q)] \quad (42)$$

$$319 \quad + f_a \nu_y (x_{NR} \sin \theta_t + z_{NR} \cos \theta_t) \quad (43)$$

$$320 \quad + f_a \cos(\theta_t + \nu_y q) \quad (44)$$

321 Details on the derivations are given in Appendix E1. The mass matrix consists of three main contributions: Equation 37
 322 represents the elastic mass and the rotor nacelle assembly (RNA) mass, Equation 38 is the generalized rotational inertia of the
 323 RNA, and Equation 39 is the inertial coupling between the tower bending and the rotation of the nacelle. The forcing terms
 324 are identified as follows: Equation 40 consists of the elastic load resulting from the external forces on the tower, the elastic and
 325 geometric stiffness loads, and the damping load on the tower; Equation 41 is the gravitational load from the RNA, which will

326 contribute to the stiffness of the system; Equation 42 is the centrifugal force of the RNA (“ $M\omega^2r$ ” with $\omega = \nu_y \dot{q}$); Equation 43
 327 is the generalized torque from the aerodynamic thrust; and Equation 44 is the thrust contribution acting directly along the
 328 direction of the shape function degree of freedom (along x). The RNA center of mass plays an important part in the equations
 329 (see the terms $(M_N x_{NG} + M_R x_{NR})$ and $(M_N z_{NG} + M_R z_{NR})$).

330 The equations of motion given in Equation 36 can be used to perform time domain simulations of a wind turbine. It is noted
 331 that the two degrees of freedom are only coupled by the aerodynamic loads. The nonlinear model was used in previous work
 332 for time domain simulations and its linear version was used for state estimations (Branlard et al., 2020a, b). In this section,
 333 we apply the linearized form to compute the natural frequency of the turbine tower fore-aft mode. The linearized stiffness is
 334 obtained by taking the gradient of the forcing with respect to q , and using a small angle approximation for ν_y to the second
 335 order:

$$336 \quad K_{q,lin} = (K_e + K_g) - \nu_y^2 g (M_N z_{NG} + M_R z_{NR} - f_a q \cos \theta_t) + \nu_y f_a \sin \theta_t \quad (45)$$

337 For the NREL 5-MW reference turbine (Jonkman et al., 2009), the different numerical values are: $g = 9.807 \text{ m} \cdot \text{s}^{-2}$, $\theta_t = 5$
 338 deg, $x_{NR} = -5.0 \text{ m}$, $z_{NR} = 2.4 \text{ m}$, $L_T = 87.6 \text{ m}$, $z_{NG} = 1.75 \text{ m}$, $x_{NG} = 1.9 \text{ m}$, $M_R = 1.1e5 \text{ kg}$, $J_{x,R} = 3.86e7 \text{ kg m}^2$,
 339 $J_{\oplus,R} = 1.92e7 \text{ kg m}^2$, $M_N = 2.4e5 \text{ kg}$, $J_{y,N} = 1.01e6 \text{ kg m}^2$, $M_{RNA} = 3.5e5 \text{ kg}$. The first fore-aft shape function of the
 340 NREL 5-MW turbine tower and its derivatives are:

$$341 \quad \Phi_1(z) = (a_2 \bar{z}^2 + a_3 \bar{z}^3 + a_4 \bar{z}^4 + a_5 \bar{z}^5 + a_6 \bar{z}^6) / (a_2 + a_3 + a_4 + a_5 + a_6)$$

$$342 \quad \frac{d\Phi_1}{dz}(z) = \frac{1}{L_T} (2a_2 \bar{z} + 3a_3 \bar{z}^2 + 4a_4 \bar{z}^3 + 5a_5 \bar{z}^4 + 6a_6 \bar{z}^5) / (a_2 + a_3 + a_4 + a_5 + a_6) \quad (46)$$

$$343 \quad \frac{d^2\Phi_1}{dz^2}(z) = \frac{1}{L_T^2} (2a_2 + 6a_3 \bar{z} + 12a_4 \bar{z}^2 + 20a_5 \bar{z}^3 + 30a_6 \bar{z}^4) / (a_2 + a_3 + a_4 + a_5 + a_6)$$

344 with $\bar{z} = z/L$, $a_2 = 0.7004$, $a_3 = 2.1963$, $a_4 = -5.6202$, $a_5 = 6.2275$, and $a_6 = -2.504$. The material properties and the shape
 345 function are illustrated in Figure 5. The scaling of the shape functions given in Equation 46 is important to obtain the correct
 346 numerical values for the flexible tower, namely: $\nu_y = 0.0185$, $M_e = 5.4e4$, $K_e = 1.91e6$, $K_g = -5.2e4 - 1.0e4 = -6.20e4$,
 347 $\omega_e = \sqrt{(K_e + K_g)/M_e} = 5.85 \text{ rad/s}$. These numerical values, with $q = 0$, lead to: $M_q = 4.375e5$ and $K_q = 1.849e9$. The
 348 first fore-aft mode of the wind turbine has a natural frequency of $f = \sqrt{K_q/M_q} = 0.3272 \text{ Hz}$. This value was compared with
 349 results obtained using OpenFAST linearization. Both methods are in strong agreement, with differences only arising at the fifth
 350 decimal place.

351 4.5 Three-degrees-of-freedom model of a land-based or fixed-bottom turbine

352 We consider the same system as the one presented in subsection 4.4, but the tower is now represented by one shape function in
 353 both the fore-aft and side-side directions, $\Phi_1 = \Phi_1 e_x$ and $\Phi_2 = \Phi_2 e_y$. The degrees of freedom are $\mathbf{q} = (q_1, q_2, \psi)$, where q_1
 354 and q_2 are the generalized (elastic) coordinates in the fore-aft and side-side directions, respectively, and ψ is the rotor azimuth.
 355 A sketch of the system is given in Figure 4.

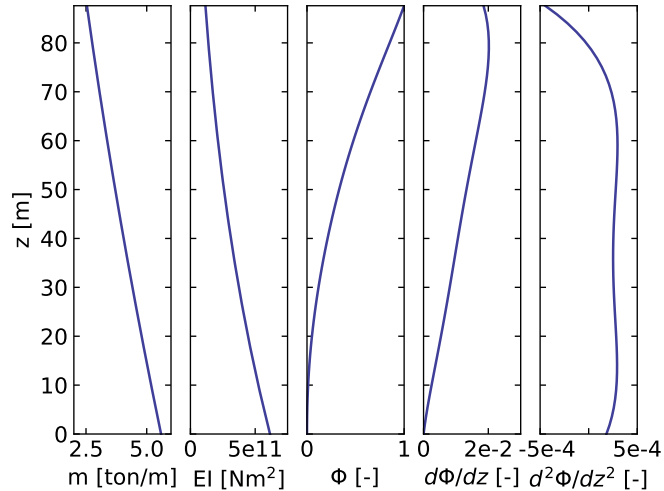


Figure 5. Properties of the NREL 5-MW turbine tower: mass per length (m), bending stiffness (EI), and shape function displacement (Φ), slope ($d\Phi/dz$) and curvature ($d^2\Phi/dz^2$).

356 The slopes of the shape functions at the tower top are key coupling parameters of the model, noted ν_x and ν_y . The aerody-
357 namic thrust and torque are noted f_a and τ_a , acting at point R . The distributed loads on the tower, p_x and p_y (from aerodynam-
358 ics and hydrodynamics), are projected against the shape functions to obtain the generalized forces $f_{e1} = \int \Phi_1 p_x dz$ and $f_{e2} =$
359 $\int \Phi_2 p_y dz$. The moments of inertia of the rotor in its coordinates are $(J_{x,R}, J_{\oplus,R}, J_{\ominus,R})$. We note that \mathbf{M}_e , \mathbf{K}_e , and \mathbf{D}_e are
360 the generalized mass, stiffness, and damping, respectively, associated with a given shape function (e.g., $M_{e11} = \int \Phi_1^2 m(z) dz$,
361 where m is the mass per length of the tower). The application of the symbolic framework leads to the equations of motion
362 given in Appendix E2. To simplify the equations and limit their length when printing them in this article, we have applied a
363 first-order small-angle approximation for θ_t , and a second-order approximation for ν_x and ν_y . It is observed from Equation E14
364 that a first-order approximation for ν_y would have removed the influence of the rotor and nacelle y -inertia on the generalized
365 mass associated with the tower fore-aft bending.

366 We performed a time simulation of the model using both our symbolic framework YAMS and OpenFAST. The time integra-
367 tion in YAMS currently relies on tools provided in the SciPy package, which implements several time integrators. A sufficient
368 level of accuracy was obtained using a fourth-order Runge-Kutta method, which is the default method. Kane's method, which
369 uses a minimal set of coordinates, tends to lead to stiff systems, and it is possible that implicit integrators may be needed for
370 other systems. We compare the time series obtained using our generated functions with results from the equivalent OpenFAST
371 simulation in Figure 6. In this simulation, the tower top is initially displaced by 1 m in the x and y directions, and the rotational
372 speed is 5 rpm. We report the mean relative error, ϵ , and the coefficient of determination, R^2 , on the figure. We observe that
373 our model is in strong agreement with the OpenFAST simulation. The differences in the second tower degree of freedom are
374 attributed to 1) the handling of the small-angle approximation, which is different in OpenFAST (using the closest orthonormal
375 matrix; Jonkman (2009)) and in our formulation (two successive rotations, linearized); 2) the nonlinear geometric corrections

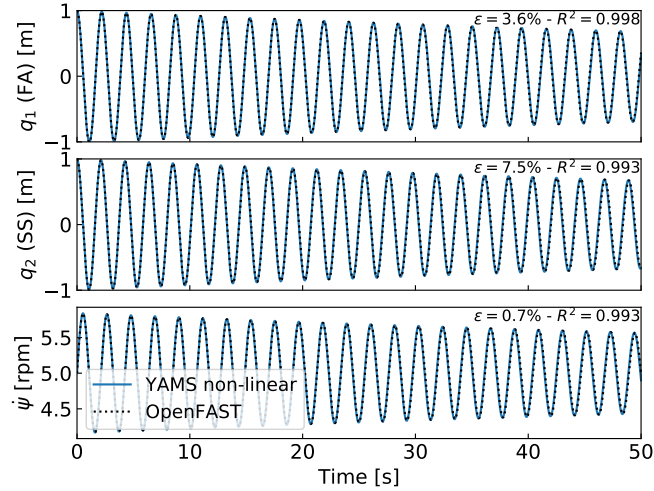


Figure 6. Free decay results for the land-based/fixed-bottom model using both the symbolic framework (YAMS) and OpenFAST. From top to bottom: tower fore-aft bending, tower side-side bending, and shaft rotational speed.

376 that are implemented in OpenFAST, which we have omitted here by only selecting shape function expansion to the zeroth order
 377 (see subsection 5.2). The variation in azimuthal speed, resulting from the coupling between the gyroscopic loads and the tower
 378 bending, is captured well.

379 4.6 Three-degrees-of-freedom model of a floating wind turbine

380 In this example, we demonstrate the applicability of the method for a floating wind turbine. We model the turbine using three
 381 bodies: rigid floater, flexible tower, and rigid RNA (labeled “N”). The degrees of freedom selected are: $\mathbf{q} = (x, \phi, q_T)$, where x
 382 is the floater surge, ϕ is the floater pitch, and q_T is the coordinate associated with a selected fore-aft shape function. A sketch
 383 of the model is given in Figure 7. The notations are similar to the ones presented in subsection 4.5. Lumped hydrodynamic
 384 loads at the floater center of mass are now added. The model can also be used for a combined tower and floater that is flexible,
 385 simply by setting the mass of the floater to zero and including the hydrodynamic loading into the loading p_x . The equations of
 386 motion are given in Appendix E3. The equations were simplified using a first-order small-angle approximation of θ_t and ϕ_y ,
 387 and a second-order approximation for ν_y .

388 We performed a numerical simulation of the model generated by YAMS and compared it with OpenFAST for a case with
 389 gravitational loads only, starting with $x = 0$ m, $\phi = 2$ deg, and $q_T = 1$ m. The results are presented in Figure 8. We observe
 390 again that the results from the two models correlate to a high degree.

391 We also compared the linearized version of both models. The symbolic framework can generate the linearized mass, stiffness,
 392 and damping matrices, as described in subsection 2.5. The matrices are then combined into a state matrix and compared with
 393 the state matrices written by the OpenFAST linearization feature. The eigenvalue analysis of the YAMS state matrix returned

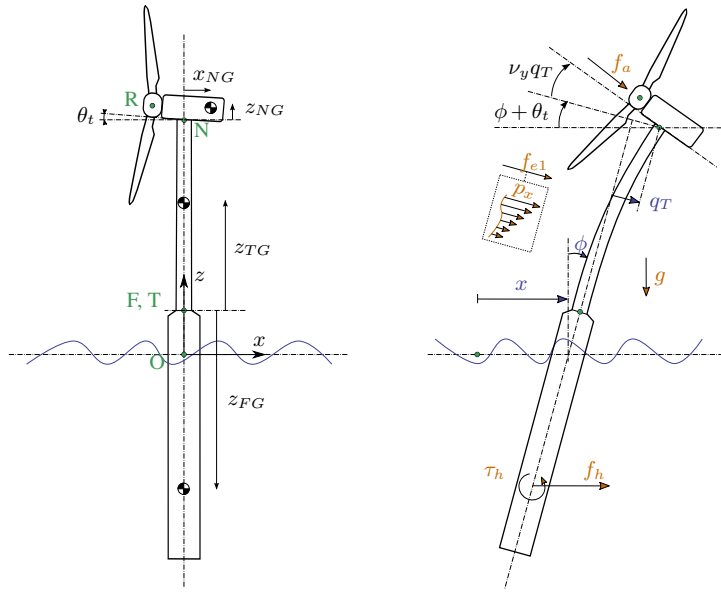


Figure 7. Model of a floating wind turbine using three degrees of freedom. Points are indicated in green, degrees of freedom in blue, and loads in orange.

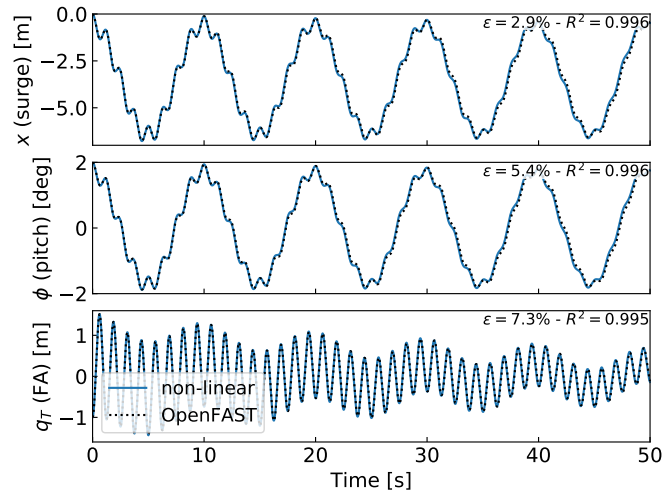


Figure 8. Free-decay results for the floating wind turbine model using YAMS and OpenFAST. From top to bottom: surge, pitch, and tower fore-aft bending.

394 a pitch and fore-aft frequencies of 0.099 Hz and 0.799 Hz, respectively, whereas OpenFAST returned 0.095 Hz and 0.795 Hz.
 395 The 4% error in the pitch frequency appears reasonable in view of the approximations used.

397 **5.1 Applications and advantages of the method**

398 The implementation of the symbolic YAMS library was originally motivated by the need to obtain a simple linearized model
399 of a floating wind turbine for frequency domain simulations. There are multiple potential applications of the framework:

- 400 – The generated equations can be used in time domain simulation tools. The equations can be readily exported to different
401 programming languages (C, FORTRAN, or Python) providing computationally efficient tools, particularly because the
402 method generates compact and minimal equations. This is in contrast to most other multibody codes, in which many
403 terms are calculated as matrix equations and through successive function calls. Further, the symbolic framework allows
404 us to generate optimized code, in which common terms and factors are computed once and stored in temporary variables
405 for reuse in the different expressions. In our examples, time domain simulations were observed to be 2 orders of mag-
406 nitude faster when using the automatically generated code in Python compared to OpenFAST simulations that rely on a
407 compiled language. Using such a framework can be considered in the future to replace the existing ElastoDyn module
408 of OpenFAST. It can also be applied to unusual configurations such as multirotor or vertical-axis turbine concepts. Ded-
409 icated code can be generated for specific applications for increased performance. For instance, implicit integrators with
410 iterative Newton-Raphson-like solvers benefit from the possibility of generating exact and efficient Jacobians along with
411 the equations of motion.
- 412 – The generation of linearized models has a wide range of applications, such as linear time domain simulations, controller
413 design and tuning, frequency domain analyses, stability analyses, state observers, or digital twins. The symbolic approach
414 is severalfold faster than alternative approaches because it can be evaluated for all operating points at once, whereas other
415 methods (e.g., OpenFAST, HAWCStab2) require multiple linearization calls.
- 416 – Analytical linearization with respect to parameters is directly obtained using our tool, which can be used for sensitivity
417 analyses, parameter studies, optimizations, integrated design approaches, and controls co-design (e.g., using methods
418 such as linear-matrix-inequality-based designs) (Pöschke et al., 2020). Nonanalytical approaches require numerous lin-
419 earizations and evaluations at various operating points (Jonkman et al., 2022).
- 420 – In addition to the nonlinear or linear equations of motion in minimal coordinates, the equations for the constraint forces
421 or any auxiliary kinematic variable can also be generated efficiently by inserting unknown virtual displacements in the
422 equations (see Appendix D5 for an alternative approach). The position of all bodies in local or global coordinates can
423 be recovered from the minimal coordinates and, in combination with the flexible code generation, be used to output data
424 (e.g., for 3D animations of the turbine).
- 425 – Analytical gradients of the equations can be computed and used in optimizations, nonlinear model predictive control,
426 or moving horizon estimation. External loads that cannot be expressed analytically can be defined as generic functions

- 427 of the structural degrees of freedom, inputs, and parameters. After the code generation, the user can link a numerical
428 implementation of the function and its numerical gradients to be able to use a mix of analytical and numerical gradients.
- 429 – Another advantage of the presented method is the possibility to quickly generate models with different levels of de-
430 tail, ensuring consistency between the different levels of fidelity. This is in contrast to other more heuristic modeling
431 approaches in which parameters often have to be retuned for each added degree of freedom.
 - 432 – The method provides useful insights and can be used as an educational tool: simple models of a system with few degrees
433 of freedom can readily be obtained, studied, and compared to hand-based calculation.

434 **5.2 Advanced consideration**

435 Section 2 addressed the systematic derivation of the equations of motion for an assembly of rigid or flexible bodies. Some
436 advanced aspects of the method are discussed here:

- 437 – The different terms involved in the equations of motion of flexible bodies can be decomposed using shape integrals (see
438 Appendix D3). Our framework readily supports this optional decomposition: it is the responsibility of the user to provide
439 the terms and values of the expansion when numerical evaluation is to occur.
- 440 – The definition of geometric stiffening requires attention in the general case. It is accounted for by the term k_σ , presented
441 in Appendix A. We discuss geometric stiffening in more detail in Appendix C.
- 442 – The treatment of external loads was not addressed in detail in this article because the loads are application-specific (aero-
443 dynamics, hydrodynamics, etc.). The framework can accept external loads as arbitrary functions of multiple variables or
444 as analytical expressions. In the former case, the user will have to provide an implementation of the function during the
445 execution.
- 446 – Even though the equations of motion are void of constraint forces, the values of these forces can be recovered. They
447 can be expressed as functions of the external forces and the states of the system. It is not necessary to compute them by
448 iteratively solving constraint equations.
- 449 – The framework can easily include rheonomous constraints—for instance, for the pitch angle—without having to supply
450 a dedicated torque. Pitch speed and accelerations can be directly introduced into the mechanical system if they are
451 provided by a generic second-order pitch actuator model.

452 **5.3 Limitations**

453 In spite of the advantages listed in subsection 5.1, the symbolic procedure presented in this work has some potential limitations:

- 454 – Constraints and closed loops have currently not been added to the framework. The SymPy mechanics package supports
455 additional constraint equations within Kane’s method. We therefore hope that this limitation can be lifted in the future.

456 – Large problems may challenge a symbolic calculation package: memory impact, calculation time, simplification times,
457 and size of expressions may become significant. Some of these issues may be alleviated by introducing intermediate
458 variables that are only substituted for in the numerical implementation or by using a recursive formulation of the solution
459 procedure (Branlard, 2019).

460 We further note that the shape function approach is an approximate method: it introduces a separation of space and time early
461 on in the development of the nonlinear equations of motion, and applies low order polynomial (usually linear or quadratic)
462 approximations to eliminate high-order terms (see e.g. Table 1 of Wallrapp (1994)). This was presented as an advantage
463 in subsection 5.1 because the equations are obtained in compact form and are readily linearized. Yet, the approximations
464 introduced by the method may imply that nonlinearities are not well captured, which is why the models are labeled as “mid-
465 fidelity” throughout this article. The domain of validity of the nonlinear or linear models presented may therefore be limited in
466 time and space as opposed to fully nonlinear methods. Advanced methods to obtain high-fidelity reduced-order models from
467 nonlinear dynamic systems are beyond the scope of this work, see, e.g. Steindl and Troger (2001); Benner et al. (2015); Touzé
468 et al. (2021).

469 **6 Conclusions**

470 We presented a symbolic framework to obtain the linear and nonlinear equations of motion of a multibody system made of
471 rigid bodies, flexible bodies, and kinematic joints. Our approach is based on Kane’s method and a nonlinear shape function
472 representation of flexible bodies. We provided different wind energy examples and verified the results against OpenFAST
473 simulations. The framework can readily provide models suitable to a wide range of applications with competitive computational
474 times. The framework is open source, and the examples presented are available in the repository. Future work will focus on
475 applying the framework to dedicated research projects, with more complex systems, and potentially extend the framework to
476 account for closed-loop systems and arbitrary constraints.

477 *Author contributions.* Both authors exchanged over the last two years about the implementation of such a framework and its application to
478 wind energy. EB wrote a Python implementation and JG wrote a Maxima implementation. EB wrote the main corpus of the article, with
479 feedback and contributions from JG.

480 *Competing interests.* No competing interests are present.

481 *Code availability.* A Zenodo link will be created for <https://github.com/ebanlard/yams>. The examples given in this articles are found in the
482 folder `welib/yams/papers` of the repository.

483 *Acknowledgements.* This work was authored in part by the National Renewable Energy Laboratory, operated by Alliance for Sustainable
 484 Energy, LLC, for the U.S. Department of Energy (DOE) under Contract No. DE-AC36-08GO28308. Funding provided by U.S. Department
 485 of Energy Office of Energy Efficiency and Renewable Energy Wind Energy Technologies Office. The views expressed in the article do
 486 not necessarily represent the views of the DOE or the U.S. Government. The U.S. Government retains and the publisher, by accepting the
 487 article for publication, acknowledges that the U.S. Government retains a nonexclusive, paid-up, irrevocable, worldwide license to publish or
 488 reproduce the published form of this work, or allow others to do so, for U.S. Government purposes.

489 *Financial support.* This work was funded under the Technology Commercialization Fund Project, supported by the DOE's Wind Energy
 490 Technologies Office.

491 **Appendix A: Equations for a flexible body and shape integrals**

492 In this section, we detail the equations of motion of a flexible body. The reader is referred to the following references for a complete treatment
 493 of the equations of motion: Shabana (2013), Schwertassek and Wallrapp (1999), and Wallrapp (1994). The subscript i , indicating the body
 494 index, is dropped. All quantities (vectors and matrices) are expressed in the body frame of reference; therefore, the prime notation is also
 495 dropped in this section. The number of flexible shape functions associated with the body is n_e , the flexible degrees of freedom are \mathbf{q}_e , and
 496 the shape functions are gathered into a matrix Φ of size $(3 \times n_e)$. The equations of motion, given in Equation 11, are repeated below:

$$497 \begin{bmatrix} M_{xx} & M_{x\theta} & M_{xe} \\ & M_{\theta\theta} & M_{\theta e} \\ \text{sym.} & & M_{ee} \end{bmatrix} \begin{bmatrix} \mathbf{a}_i \\ \dot{\boldsymbol{\omega}}_i \\ \ddot{\mathbf{q}}_e \end{bmatrix} + \begin{bmatrix} \mathbf{k}_{\omega,x} \\ \mathbf{k}_{\omega,\theta} \\ \mathbf{k}_{\omega,e} \end{bmatrix} + \begin{bmatrix} 0 \\ 0 \\ \mathbf{k}_e \end{bmatrix} = \begin{bmatrix} \mathbf{f}_x \\ \mathbf{f}_\theta \\ \mathbf{f}_e \end{bmatrix} \quad (\text{A1})$$

498 The different terms of the mass matrix are obtained as follows:

$$499 M_{xx} = \int \mathbf{I}_3 dm = M \mathbf{I}_3 \quad (3 \times 3) \quad (\text{A2})$$

$$500 M_{x\theta} = - \int \tilde{\mathbf{s}}_P dm = -M \tilde{\mathbf{s}}_{CM} \quad (3 \times 3) \quad (\text{A3})$$

$$501 M_{\theta\theta} = - \int \tilde{\mathbf{s}}_P \tilde{\mathbf{s}}_P^T dm = \mathbf{J} \quad (3 \times 3) \quad (\text{A4})$$

$$502 M_{\theta e} = \int \tilde{\mathbf{s}}_P \Phi dm = \mathbf{C}_r^T \quad (3 \times n_e) \quad (\text{A5})$$

$$503 M_{xe} = \int \Phi dm = \mathbf{C}_t^T \quad (3 \times n_e) \quad (\text{A6})$$

$$504 M_{ee} = \int \Phi^T \Phi dm \quad (n_e \times n_e) \quad (\text{A7})$$

505 The integrals are volume integrals over the volume of the body (for beams, they reduce to line integrals). The notation $[\tilde{\cdot}]$ represents the skew
 506 symmetric matrix. M is the mass of the body. The vector \mathbf{s}_{CM} is the vector from the origin of the body to undeflected center or mass (CM)
 507 of the body. The notations \mathbf{C}_t ($n_e \times 3$) and \mathbf{C}_r ($n_e \times 3$) are introduced to match Wallrapp's notations. The vector \mathbf{s}_P is the vector from
 508 the origin of the body to a deflected point of the body of elementary mass dm . The undeflected position of this point is written as \mathbf{s}_{P_0} and
 509 the displacement field \mathbf{u} , such that: $\mathbf{s}_P = \mathbf{s}_{P_0} + \mathbf{u}$. Typically, the displacement field is given by $\mathbf{u} = \Phi \mathbf{q}_e$, but a higher-order expansion can
 510 also be introduced (see Wallrapp (1994) and Appendix D4). Wallrapp also includes the elementary mass moment of inertia, which results in

511 additional terms in the integrals (see Wallrapp (1994)). Such contributions are relevant, for instance, when considering the torsion of a beam
512 (see Branlard (2019)). The block matrices M_{xx} , M_{xe} , and M_{ee} do not depend on the deformation of the body and are therefore constant.
513 The other terms are functions of \mathbf{q}_e . They may be expressed as linear combinations of constant integrals (see Appendix D3).

514 The quadratic velocity terms, \mathbf{k}_ω , are given as:

$$515 \quad \mathbf{k}_{\omega,x} = 2\tilde{\omega}\mathbf{C}_t^T\dot{\mathbf{q}}_e + M\tilde{\omega}\tilde{\omega}\mathbf{s}_{CM} \quad (3 \times 1) \quad (\text{A8})$$

$$516 \quad \mathbf{k}_{\omega,\theta} = \tilde{\omega}M_{\theta\theta}\boldsymbol{\omega} + \left[\sum_{j=1..n_e} \mathbf{G}_{r,j}\dot{q}_{e,j} \right] \boldsymbol{\omega} \quad (3 \times 1) \quad (\text{A9})$$

$$517 \quad \mathbf{k}_{\omega,e} = \left[\boldsymbol{\omega}^T \mathbf{O}_{e,j} \boldsymbol{\omega} \right]_{j=1..n_e} + \left[\sum_{j=1..n_e} \mathbf{G}_{e,j}\dot{q}_{e,j} \right] \boldsymbol{\omega} \quad (n_e \times 1) \quad (\text{A10})$$

518 where

$$519 \quad \mathbf{G}_{r,j} = -2 \int \tilde{\mathbf{s}}_P \tilde{\boldsymbol{\Phi}}_j \, dm \quad (3 \times 3) \quad (\text{A11})$$

$$520 \quad \mathbf{O}_{e,j} = \int \tilde{\boldsymbol{\Phi}}_j \tilde{\mathbf{s}}_P \, dm = -\frac{1}{2} \mathbf{G}_{r,j}^T \quad (3 \times 3) \quad (\text{A12})$$

$$521 \quad \mathbf{G}_{e,j} = -2 \int \boldsymbol{\Phi}^T \tilde{\boldsymbol{\Phi}}_j \, dm \quad (n_e \times 3) \quad (\text{A13})$$

522 The first term of Equation A10 is obtained by vertically stacking the contribution of each shape function. In the standard input data format,
523 this term is reshaped as the product $\mathbf{O}_e\boldsymbol{\Omega}$, where:

$$524 \quad \mathbf{O}_e = [O_{e,j,11}, O_{e,j,22}, O_{e,j,33}, O_{e,j,12} + O_{e,j,21}, O_{e,j,23} + O_{e,j,32}, O_{e,j,13} + O_{e,j,31}]_{j=1..n_e} \quad (n_e \times 6) \quad (\text{A14})$$

$$525 \quad \boldsymbol{\Omega} = [\omega_x^2, \omega_y^2, \omega_z^2, \omega_x\omega_y, \omega_y\omega_z, \omega_x\omega_z] \quad (6 \times 1) \quad (\text{A15})$$

526 The body elastic forces are given by:

$$527 \quad \mathbf{k}_e = \mathbf{k}_\sigma + \mathbf{K}_e \mathbf{q}_e + \mathbf{D}_e \dot{\mathbf{q}}_e \quad (\text{A16})$$

528 where \mathbf{K}_e and \mathbf{D}_e are the elastic stiffness and damping matrices, and \mathbf{k}_σ represents geometric stiffening terms (see Appendix C). The elastic
529 damping forces are often given as stiffness proportional damping. For more details, see Wallrapp (1994), and for more examples with elastic
530 beams, see Branlard (2019). The external loads can be assumed to consist of distributed volume forces, \mathbf{p} (in practice they are primarily
531 surface forces or line forces), and a gravitational acceleration field, \mathbf{g} . The components of the external loads in Equation A1 are then obtained
532 by integration over the whole body:

$$533 \quad \mathbf{f}_x = \int \mathbf{p} \, dV + M_{xx}\mathbf{g} \quad (3 \times 1) \quad (\text{A17})$$

$$534 \quad \mathbf{f}_\theta = \int \mathbf{s}_P \times \mathbf{p} \, dV + M_{\theta x}\mathbf{g} \quad (3 \times 1) \quad (\text{A18})$$

$$535 \quad \mathbf{f}_e = \int \boldsymbol{\Phi}^T \mathbf{p} \, dV + M_{ex}\mathbf{g} \quad (n_e \times 1) \quad (\text{A19})$$

536 Appendix B: Application of the shape function approach to an isolated beam

537 In this section, we illustrate how the elastic equations of Appendix A can be applied to an isolated beam. Examples of applications are further
538 given in subsection 4.3 and subsection 4.4. We consider a beam directed along the z -axis and bending in the x and y directions. Expressions

539 are written in the coordinate system of the beam and primes are dropped in this section. The beam properties are the following: length, L ,
540 mass per length, m , and bending stiffness, EI_x and EI_y . We assume that the displacement field is such that the shape functions are functions
541 of z only: $\mathbf{u}(z, t) = \sum_{i=1}^{n_e} \Phi_i(z) q_{e,i}(t)$. We also assume that the shape functions satisfy at least the geometric boundary conditions. The
542 kinetic energy of the beam is $T = \frac{1}{2} \int_0^L m \dot{\mathbf{u}}^2 dz = \frac{1}{2} \sum_i \sum_j M_{e,ij} \dot{q}_{e,j} \dot{q}_{e,i}$, where $M_{e,ij}$ is (see Equation A7):

$$543 \quad M_{e,ij} = \int_0^L m(z) \Phi_i(z) \cdot \Phi_j(z) dz, \quad i, j = 1, \dots, n_e \quad (\text{B1})$$

544 Equation B1 involves a scalar product of the shape functions at each spanwise position. Integrals over the moment of inertia can be used
545 to account for torsion (see Branlard (2019)). The potential energy (strain energy) of the beam, is obtained as $V = \frac{1}{2} \sum_i \sum_j K_{e,ij} q_{e,i} q_{e,j}$,
546 where $K_{e,ij}$ are the elements of the stiffness matrix, which, under the assumption of small deformations, are given by:

$$547 \quad K_{e,ij} = \int_0^L \left[EI_y \frac{d^2 \Phi_{i,x}}{dz^2} \frac{d^2 \Phi_{j,x}}{dz^2} + EI_x \frac{d^2 \Phi_{i,y}}{dz^2} \frac{d^2 \Phi_{j,y}}{dz^2} \right] dz, \quad i, j = 1, \dots, n_e \quad (\text{B2})$$

548 Elongation and torsional strains (EA and GK_t) can similarly be added to the strain energy and the stiffness matrix if longitudinal and
549 torsional displacement fields are included in the shape functions. The external loads on the beam are assumed to consist of a distributed force
550 vector, $\mathbf{p}(z)$. The virtual work done by the force \mathbf{p} for each virtual displacement $\delta q_{e,i}$ provides the generalized force as (see Equation A17):

$$551 \quad f_{e,i} = \int_0^L \Phi_i \cdot \mathbf{p} dz \quad (\text{B3})$$

552 The equations of motion of the isolated beam and then written in matrix form as:

$$553 \quad \mathbf{M}_e \ddot{\mathbf{q}}_e + \mathbf{D}_e \dot{\mathbf{q}}_e + \mathbf{K}_e \mathbf{q}_e = \mathbf{f}_e \quad (\text{B4})$$

554 where $\mathbf{q}_e = [q_{e,1}, \dots, q_{e,n}]$. Damping is typically added a posteriori to the equations, where the Rayleigh damping assumption is often used:
555 $\mathbf{D}_e = \alpha \mathbf{M}_e + \beta \mathbf{K}_e$ (stiffness proportional damping implies $\alpha = 0$). If the shape functions are mode shapes, then the shape functions are
556 orthogonal, the mass and stiffness matrices are diagonal, and the stiffness values would be $K_{e,ii} = \omega_{e,i}^2 M_{e,ii}$, with $\omega_{e,i} = \sqrt{K_{e,ii}/M_{e,ii}}$
557 the eigenfrequency of the beam mode i . The modal damping is then given by $D_{e,ii} = 2\zeta_i M_{e,ii} \omega_{e,i}$, where ζ_i is the damping ratio associated
558 with mode i .

559 If the beam is loaded axially by a force $N(z)$ (assumed to be independent of the elastic degrees of freedom), then this force produces a
560 distributed load in the transverse direction equal to $\mathbf{n} = \frac{\partial}{\partial z} [N(z) \frac{\partial \mathbf{u}}{\partial z}]$, with components in the y and z directions (see Branlard (2019)). The
561 generalized force associated with this loading is then $Q_{N,i} = \int_0^L \Phi_i \cdot \mathbf{n} dz$. Inserting the expression of \mathbf{n} and \mathbf{u} , the generalized force has
562 the form of a stiffness term: $Q_{N,i} = -\sum_j K_{N,ij} q_{e,j}$ with

$$563 \quad K_{N,ij} = -\int_0^L \Phi_i \cdot \frac{d}{dz} \left[N(z) \frac{d\Phi_j}{dz} \right] dz = \int_0^L N(z) \frac{d\Phi_i}{dz} \cdot \frac{d\Phi_j}{dz} - \left[N(z) \Phi_i \cdot \frac{d\Phi_j}{dz} \right]_0^L \quad (\text{B5})$$

564 and where integration by parts was used to obtain the second equality. Examples of applications are given in subsection 4.3 and subsection 4.4.
565 The fact that an axial load leads to a stiffness term is referred to as ‘‘geometric stiffness,’’ which is the topic of Appendix C.

566 Appendix C: Geometric stiffness

567 C1 General treatment

568 Geometric stiffness refers to the apparent change of stiffness of a structure depending on the loading it is subject to. In this section, we present
 569 a linear formulation of geometric stiffness for a flexible body undergoing motion and subject to arbitrary loading, inspired by Schwertassek
 570 and Wallrapp (1999). Additional details may be found in Wallrapp and Schwertassek (1991). The main component of the geometric stiffening
 571 term \mathbf{k}_σ can be written:

$$572 \quad \mathbf{k}_\sigma = \mathbf{K}_g \mathbf{q}_e \tag{C1}$$

573 where \mathbf{K}_g is the geometric stiffness matrix of shape $n_e \times n_e$. In general, this matrix is time-dependent, as it is a function of the inertial and
 574 external loads acting on the body. The inertial loads consist of contributions from the linear acceleration, \mathbf{a} , rotational acceleration, $\dot{\boldsymbol{\omega}}$, and
 575 cross products of the rotational velocity of the body (centrifugal and gyroscopic terms). The external loads consist of the gravitational force,
 576 distributed forces per unit length, \mathbf{p} , point loads, \mathbf{F}^k , and point moments, $\boldsymbol{\tau}^k$, where k is the node index where the point loads are applied.
 577 Each of these contributions can be computed at each time step using a linear superposition of unit geometric stiffness matrices, noted \mathbf{K}_{g*} ,
 578 as follows:

$$579 \quad \mathbf{K}_g = \sum_{\alpha=1}^3 [(a_\alpha - g_\alpha) \mathbf{K}_{gt,\alpha} + \dot{\omega}_\alpha \mathbf{K}_{gr,\alpha}] + \sum_{\alpha=1}^3 \sum_{\beta=1}^3 \omega_\alpha \omega_\beta \mathbf{K}_{g\omega,\alpha\beta}$$

$$580 \quad + \sum_{\alpha=1}^3 \left[p_\alpha \mathbf{K}_{gp,\alpha} + \sum_k \left(F_\alpha^k \mathbf{K}_{gF,\alpha}^k + \tau_\alpha^k \mathbf{K}_{g\tau,\alpha}^k \right) \right] \tag{C2}$$

581 where the indices α and β run on the x, y , and z coordinates of the body reference frame. The matrices $\mathbf{K}_{g*,\alpha}$ or $\mathbf{K}_{g*,\alpha\beta}$ have the shape
 582 $n_e \times n_e$ and are obtained as the geometric stiffness matrices for unit accelerations, loads, or products of rotational velocities in the given
 583 direction defined by α and β (x, y , or z). For instance, $\mathbf{K}_{gt,z}$ is the geometric stiffness matrix corresponding to a unit acceleration in the
 584 z direction, $\mathbf{K}_{g\omega,xy}^k$ is the geometric stiffness matrix corresponding to a unit gyration about the x and y directions (centrifugal effect), and
 585 $\mathbf{K}_{gF,x}^k$ is the geometric stiffness matrix corresponding to a unit force in the x direction applied at the node k along the body. The effect of
 586 the Coriolis force is not mentioned in the work of Schwertassek and Wallrapp and not explicitly accounted for in Equation C2. The Coriolis
 587 force, $2m(z)\boldsymbol{\omega} \times (\sum_j \Phi_j(z) \dot{\mathbf{q}}_{e,j})$, is proportional to $\dot{\mathbf{q}}_e$. Because the instantaneous beam slope is proportional to \mathbf{q}_e , the geometric stiffening
 588 term consists of terms of the form $q_{e,j} \dot{q}_{e,k}$. In Table 1 of Wallrapp (1994), it is stated that nonlinear terms of the form $q_{e,j} \dot{q}_{e,k}$ are neglected.
 589 Yet, if the steady state deflection \mathbf{q}_e is significant, then the influence of the Coriolis term on the geometric stiffening may be significant. The
 590 effect can be included as an additional term in Equation C1 that is a function of \mathbf{q}_e and $\dot{\mathbf{q}}_e$ (expressions are provided in subsection C2). We
 591 note that the terms \mathbf{K}_{g*} have different units; for instance, the terms $\mathbf{K}_{gt,*}$ are expressed in $\text{N} \cdot \text{s}^2 \cdot \text{m}^{-2}$.

592 C2 Expressions for a beam directed along z

593 The expression for each of these matrices are given in Schwertassek and Wallrapp (1999) in the context of the finite-element method. The
 594 general expressions for a shape function approach would be beyond the scope of this article, but we provide the expressions for a beam
 595 below.

596 We adopt the same notations as Appendix B to describe the flexible beam. Following the developments that led to Equation B5, the
 597 geometric correction associated with an axial load N , is given by the generalized force:

$$598 \quad k_{\sigma,N,i} = \int_0^L N(z) \Phi_i \cdot \left[\sum_j \frac{d\Phi_j}{dz} q_j \right] dz \quad (C3)$$

599 When the axial load is not a function of the degrees of freedom, this expression can be expressed as a stiffness matrix, as indicated in
 600 Equation B5. The different unit geometric matrices introduced in Appendix C can be determined using a form of Equation B5, where the
 601 axial load N is replaced by the unit inertial or external load. Since the beam is directed along the z direction, we focus on the terms where
 602 the loads act in the z direction, all other terms being zero or negligible. The ij -component of the matrix $\mathbf{K}_{gt,z}$ is obtained by considering a
 603 unit vertical acceleration:

$$604 \quad K_{gt,z,ij} = \int_0^L N(z) \frac{d\Phi_i}{dz} \cdot \frac{d\Phi_j}{dz} dz, \quad N(z) = \int_z^L m(z) dz \quad (C4)$$

605 We write z_k the coordinate of node k along the beam. The ij -component of the matrix $\mathbf{K}_{gF,z}^k$ is obtained as:

$$606 \quad K_{gF,z,ij}^k = \int_0^L N(z) \frac{d\Phi_i}{dz} \cdot \frac{d\Phi_j}{dz} dz, \quad N(z) = 1 \text{ if } z < z_k, 0 \text{ otherwise} \quad (C5)$$

607 The ij -component of the matrix $\mathbf{K}_{g\omega,\alpha\beta}$ is obtained by considering unit centrifugal loads generated using independent rotations around the
 608 unit vectors e_x , e_y , and e_z :

$$609 \quad K_{g\omega,\alpha\beta,ij} = \int_0^L -e_z \cdot (\tilde{e}_\alpha \tilde{e}_\beta N(z)) \frac{d\Phi_i}{dz} \cdot \frac{d\Phi_j}{dz} dz, \quad N(z) = \int_z^L m(z) s_{P_0} dz \quad (C6)$$

610 Similarly, the ij -component of the matrix $\mathbf{K}_{gr,\alpha}$ is:

$$611 \quad K_{gr,\alpha,ij} = \int_0^L -e_z \cdot (\tilde{e}_\alpha N(z)) \frac{d\Phi_i}{dz} \cdot \frac{d\Phi_j}{dz} dz, \quad N(z) = \int_z^L m(z) s_{P_0} dz \quad (C7)$$

612 The Coriolis force, $2m(z)\omega \times (\sum_j \Phi_j(z)\dot{q}_{e,j})$, can also have an axial contribution. Using Equation C3, the generalize force is:

$$613 \quad k_{\sigma,\text{Cor},i} = \int_0^L N(z) \Phi_i \cdot \left[\sum_j \frac{d\Phi_j}{dz} q_j \right] dz, \quad N(z) = 2 \int_z^L m(z) \sum_k [\omega_x \Phi_{k,y}(z) - \omega_y \Phi_{k,x}(z)] \dot{q}_k dz \quad (C8)$$

614 Equation C8 may be rearranged by introducing a three-dimensional tensor made of shape integrals that are independent of the elastic degrees
 615 of freedom and the rotational speed, and therefore speedup the evaluation of this expression at each time step. The vector $\mathbf{k}_{\sigma,\text{Cor}}(\mathbf{q}_e, \dot{\mathbf{q}}_e)$ is
 616 added to the right hand side of Equation C1.

617 C3 Integration into the equations of motion

618 The term $\mathbf{k}_\sigma = \mathbf{K}_g \mathbf{q}_e$ appears on the third block-row of the equations of motion of the flexible body (Equation A1). Because of the linearity
 619 with respect to the acceleration, rotational velocities, and forces, the different contributions can optionally be incorporated into the third
 620 block-row of the mass matrix (\mathbf{M}_{e*}), the term $\mathbf{k}_{\omega,e}$, and the term \mathbf{f}_e , respectively. For instance, the term $\sum a_\alpha \mathbf{K}_{gt,\alpha} \mathbf{q}_e$ can be reorganized
 621 as $[\mathbf{K}_{gt}] \mathbf{q}_e \cdot \mathbf{a}$ (using loose notations); therefore, the mass matrix can be updated such that \mathbf{M}_{xe} becomes $\mathbf{M}_{xe} + [\mathbf{K}_{gt}] \mathbf{q}_e$. When a Taylor
 622 expansion is used, such integration is easily implemented as a first-order term (see Appendix D3).

623 Appendix D: Alternative formulations

624 Different formulations of flexible multibody dynamics using shape functions are found in the literature. Some of the alternatives are briefly
625 discussed in this section.

626 D1 Jacobian and velocity transformation matrix

627 In Equation 7, the Jacobian terms \mathbf{J} and the virtual work are expressed in vector form. In such form, there is no need to state in which coordi-
628 nate system the different vectors are expressed. This is convenient to reduce the size of the expressions when using symbolic calculations. In
629 a numerical framework, the vector will have to be expressed in a common frame. When such an approach is used (see, e.g., Lemmer (2018);
630 Branlard (2019)), the Jacobians are sometimes stacked into a matrix form:

$$631 \mathbf{J} = \begin{bmatrix} \mathbf{J}_v \\ \mathbf{J}_\omega \\ \mathbf{J}_e \end{bmatrix} \quad (D1)$$

632 Some implementation choices are needed depending if these matrices are expressed in the global frame or a body frame. The Jacobian
633 matrices are referred to as “velocity transformation matrix,” and the link between formulations in global and local coordinates is given in
634 Branlard (2019). In the same reference, recursive relationships are given for tree-like assembly of bodies to help express the Jacobian matrices
635 of each body recursively, based on the matrices of the parent body. It is also noted that the quadratic velocity terms, \mathbf{k}_ω , can be obtained
636 using the time derivative of the Jacobian matrix.

637 D2 Rotations and torsion

638 In this article, we have not elaborated on the change of orientation introduced by shape functions. In most applications, bodies are connected
639 at their extremities and the deflection slope at a body extremity will induce a rotation of the subsequent body (e.g., tilting and rolling of
640 the nacelle at the tower top). The deflection slope can be obtained from the knowledge of the shape functions. This is readily accounted
641 for by introducing a time-varying rotation matrix between bodies, and this is the approach used in our symbolic framework. A formalism
642 of rotations of bodies connected at their extremities is given in Branlard (2019). A more general formulation, introducing shape function
643 rotations Ψ , is given in (Wallrapp, 1994; Schwertassek and Wallrapp, 1999; Lemmer, 2018). In such a formulation, the linear rotation field
644 is obtained as $\mathbf{I} + \widetilde{\Psi}\mathbf{q}$, where \mathbf{I} is the identity matrix.

645 D3 Shape integrals and Taylor expansion

646 The results presented in Appendix A consist of integrals over the displaced points of the structure, $\mathbf{s}_P = \mathbf{s}_{P_0} + \mathbf{u}$, where the displacement
647 field is $\mathbf{u} = \Phi\mathbf{q}_e$. The undeflected position of the structure (\mathbf{s}_{P_0}) is constant, and the shape functions are known at the initialization; the only
648 time-varying terms are the degrees of freedom \mathbf{q}_e . Therefore, the integrals can be precomputed by decomposing them into a constant part
649 and a part that is linear with respect to the degrees of freedom \mathbf{q}_e . The precomputed integrals are referred to as “shape integrals.” For a given
650 term \mathbf{T} (standing, for instance, for $\mathbf{M}_{\theta,\theta}$, \mathbf{C}_t , \mathbf{C}_r , \mathbf{G}_r , \mathbf{G}_e , or \mathbf{O}_e), the shape integral expansion is:

$$651 \mathbf{T}(\mathbf{q}_e) = \mathbf{T}^0 + \sum_{j=1..n_e} \mathbf{T}_j^1 q_{e,j} \quad (D2)$$

652 If \mathbf{T} is an array, \mathbf{T}^0 and \mathbf{T}_j^1 have the same shape as \mathbf{T} . As an example, the application of the shape integral expansion to the term $\mathbf{M}_{x\theta}$ (see
 653 Equation A3) gives:

$$654 \quad \mathbf{M}_{x\theta} = - \int \tilde{\mathbf{s}}_{P_0} dm = \mathbf{M}_{x\theta}^0 + \sum_{j=1..n_e} \mathbf{M}_{x\theta,j}^1 q_{e,j} \quad (\text{D3})$$

655 with

$$656 \quad \mathbf{M}_{x\theta}^0 = - \int \tilde{\mathbf{s}}_{P_0} dm, \quad \mathbf{M}_{x\theta,j}^1 = - \int \tilde{\Phi}_j dm \quad (\text{D4})$$

657 The zeroth- and first-order shape integrals always consist of integrals over the components of \mathbf{s}_{P_0} and Φ , which can be precomputed for a
 658 given flexible body. We note that the precomputed shape integrals can in turn be obtained from intermediate integrals (e.g., the S_* and N_*
 659 terms introduced by Wallrapp (Wallrapp, 1994), or the σ , Σ , Υ , Ψ terms introduced by Shabana (Shabana, 2013)). The zeroth- and first-order
 660 shape integrals are stored using a ‘‘Taylor’’ object-oriented class in the standard input data format defined by Wallrapp. The YAMS library
 661 can compute the shape integrals using a direct integration or using a finite-element formulation (see Schwertassek and Wallrapp (1999)).

662 The geometric stiffness introduced in Appendix C is linear in the elastic degrees of freedom q_e . Therefore, the unit geometric stiffness
 663 matrices (which are also shape integrals) can be conveniently added into the first-order terms of Equation D2. For instance, if we write \mathbf{M}_{ex}
 664 (given in Equation A6) using a first-order expansion, $\mathbf{M}_{ex} = \mathbf{M}_{ex}^0 + \mathbf{M}_{ex}^1 q_e$, then the geometric stiffening effect can directly be inserted
 665 into the first-order term, such that \mathbf{M}_{ex}^1 becomes $\mathbf{M}_{ex}^1 + \mathbf{K}_{gt}$. Similarly, the term \mathbf{K}_{gr} can be inserted into $\mathbf{M}_{\theta e}^1$, $\mathbf{K}_{g\omega}$ into \mathbf{O}_e^1 , \mathbf{K}_{gF} into
 666 Φ^1 , and $\mathbf{K}_{g\tau}$ into Ψ^1 in the calculation of the generalized forces. The different contributions are summarized in Table 6.9 of the book of
 667 Schwertassek and Wallrapp (1999). A shortcoming of inserting the geometric stiffness effects into the first-order coefficient is that it could
 668 make the mass matrix symmetric (if the user code assumes $\mathbf{M}_{xe} = \mathbf{M}_{ex}^t$), instead of acting only on the third block-row of the mass matrix.

669 **D4 Taylor expansion of the displacement field**

670 In the work of Wallrap (Wallrapp, 1993, 1994), the displacement field is assumed to be a function of the degrees of freedom, $\mathbf{u} = \Phi_u(q_e)q_e$,
 671 where Φ_u consists of a Taylor series expansion of the shape functions that contain Φ^0 and Φ^1 terms. The resulting equations of motion are
 672 still expressed using shape integrals of the form given in Equation D2, but the 1 terms will contain some additional integrals over Φ^1 . The
 673 advantage of this method is that the Φ^1 terms effectively account for the geometric stiffness. In practice, it is equivalent, and as convenient,
 674 to neglect the Φ^1 terms and introduce the geometric stiffness using the method presented in Appendix C (and optionally integrate them into
 675 the 1 terms as presented in Appendix D3).

676 **D5 ElastoDyn and the partial loads approach**

677 The ElastoDyn module of OpenFAST (Jonkman et al., 2021) uses the so-called ‘‘partial loads’’ approach to implement the equations of
 678 motion. The underlying theory used to derive the equations of motion is the same as Kane’s formalism presented in section 2, but the partial
 679 load approach takes advantage of the fact that the calculation of reaction loads or point loads at body extremities requires similar terms to the
 680 ones needed for the equations of motion. In the discussion below, we assume that the different bodies of the structure form a tree structure
 681 with the root at the bottom and the leaves above. For a tree-like structure, there is a natural relationship between loads in the structure and the
 682 degrees of freedom. A virtual displacement of a given degree of freedom will only displace the structure above it. The equation of motion
 683 of this degree of freedom can therefore be obtained from the virtual work of the loads at a point located just above the degree of freedom,
 684 as if the entire structure above was replaced by lumped loads. The point loads contain contributions from the external loads above the point
 685 in consideration, but also inertial and gyroscopic loads associated with all the degrees of freedom of the system. If the point is at a joint, the

686 loads corresponds to the reaction loads at this point. We write P the point located after a given degree of freedom r . The equation of motion
687 for this degree of freedom is obtained as if the system was isolated:

$$688 \quad \mathbf{f}_r + \mathbf{f}_r^* = 0 = \mathbf{J}_{v_{P,r}} \cdot \mathbf{f}_P + \mathbf{J}_{\omega_{P,r}} \cdot \boldsymbol{\tau}_P + h_r \quad (\text{D5})$$

689 where: $\mathbf{J}_{v_{P,r}}$ and $\mathbf{J}_{\omega_{P,r}}$ are the partial velocities of point P with respect to the degree of freedom r ; \mathbf{f}_P and $\boldsymbol{\tau}_P$ are 3-vectors containing the
690 force and torque from the structure above the degree of freedom r (including external and inertial contributions); and h_r is the generalized
691 load associated with the isolated degree of freedom r (e.g., the elastic loads for a flexible body, or the spring and damping loads for a degree
692 of freedom representing a joint). The point loads \mathbf{f}_P and $\boldsymbol{\tau}_P$ can be decomposed into terms that are proportional to the accelerations of all
693 the degrees of freedom (indexed with r) and additional terms (labeled “ t ”):

$$694 \quad \mathbf{f}_P = \sum_{j=1}^{n_q} \mathbf{f}_{P,j} \ddot{q}_j + \mathbf{f}_{P,t}, \quad \boldsymbol{\tau}_P = \sum_{j=1}^{n_q} \boldsymbol{\tau}_{P,j} \ddot{q}_j + \boldsymbol{\tau}_{P,t} \quad (\text{D6})$$

695 The terms $\mathbf{f}_{P,r}$ and $\boldsymbol{\tau}_{P,r}$ act as generalized masses and they are referred to as “partial loads”. Combining Equation D5 and Equation D6, the
696 term rj of the mass matrix and the term r of the right hand side of the equation of motion (Equation 22) are obtained as:

$$697 \quad M_{rj} = -\mathbf{J}_{v_{P,r}} \cdot \mathbf{f}_{P,j} - \mathbf{J}_{\omega_{P,r}} \cdot \boldsymbol{\tau}_{P,j}, \quad F_r = \mathbf{J}_{v_{P,r}} \cdot \mathbf{f}_{P,t} + \mathbf{J}_{\omega_{P,r}} \cdot \boldsymbol{\tau}_{P,t} + h_r \quad (\text{D7})$$

698 Therefore, the knowledge of the partial loads and the partial velocities at key points of the structure (typically, points where user outputs
699 are desired) can be used to obtain the reaction loads (Equation D6) and the equations of motion (Equation D7). This is the approach used
700 in ElastoDyn: the loads at key points of the structure were derived using hand calculations, and then the partial loads were used for the
701 implementation of the outputs and the equations of motion. The reader is referred to the notes provided in the online documentation of
702 ElastoDyn for more details (Jonkman et al., 2021). A general procedure to obtain partial loads can be devised (using kinematics to find
703 velocities and acceleration in the structure, and computing the loads from the tree top to the root), but would be beyond the scope of this
704 article.

705 **Appendix E: Equations of motion of simple wind turbine models**

706 In this section, we present the equations of motion for the examples presented in section 4.

707 **E1 Two-degrees-of-freedom model of a land-based or fixed-bottom wind turbine**

708 In this section, we provide some intermediate values to obtain the equations of motion given in subsection 4.4. We use the hat notation to
709 indicate unit vectors of a frame, where the frame is identified as t , n , r for the tower, nacelle, and rotor, respectively. For instance, $v\hat{t}_x$ is the
710 unit vector in the x direction of the tower frame. The degrees of freedom are $\mathbf{q} = (q, \psi)$. The kinematics of the tower (at its origin) are zero:

$$711 \quad \mathbf{v}_{O,T} = \mathbf{0}, \quad \boldsymbol{\omega}_T = \mathbf{0}, \quad \mathbf{a}_{O,T} = \mathbf{0} \quad (\text{E1})$$

712 All Jacobians are zero except $\mathbf{J}_{e,1T} = 1$ The inertial force, torque, and elastic force are:

$$713 \quad \mathbf{f}_T^* = C_{tTx} \ddot{q} \hat{t}_x + M_T g \hat{t}_z, \quad \boldsymbol{\tau}_T^* = C_{rTy} \ddot{q} \hat{t}_y, \quad \mathbf{E}_T^* = f_e + D_e \dot{q} + (K_e + K_q)q + M_e \ddot{q} \quad (\text{E2})$$

714 The nacelle kinematics (at its center of mass) are:

$$715 \quad \mathbf{v}_{G,N} = \dot{q}\hat{\mathbf{t}}_x + \nu_y z_{NG} \dot{q}\hat{\mathbf{n}}_x - \nu_y x_{NG} \dot{q}\hat{\mathbf{n}}_z, \quad \boldsymbol{\omega}_N = \nu_y \dot{q}\hat{\mathbf{t}}_y \quad (\text{E3})$$

$$716 \quad \mathbf{a}_{G,N} = \ddot{q}\hat{\mathbf{t}}_x + (-\nu_y^2 x_{NG} \dot{q}^2 + \nu_y z_{NG} \ddot{q})\hat{\mathbf{n}}_x + (-\nu_y^2 z_{NG} \dot{q}^2 - \nu_y x_{NG} \ddot{q})\hat{\mathbf{n}}_z \quad (\text{E4})$$

717 The Jacobians with respect to q are:

$$718 \quad \mathbf{J}_{v,1N} = \hat{\mathbf{t}}_x + \nu_y z_{NG} \hat{\mathbf{n}}_x - \nu_y x_{NG} \hat{\mathbf{n}}_z, \quad \mathbf{J}_{\omega,1N} = \nu_y \hat{\mathbf{t}}_y \quad (\text{E5})$$

719 The inertial force and torque on the nacelle are:

$$720 \quad \mathbf{f}_N^* = M_N \ddot{q}\hat{\mathbf{t}}_x + M_N (-\nu_y^2 x_{NG} \dot{q}^2 + \nu_y z_{NG} \ddot{q})\hat{\mathbf{n}}_x + M_N (-\nu_y^2 z_{NG} \dot{q}^2 - \nu_y x_{NG} \ddot{q})\hat{\mathbf{n}}_z, \quad \boldsymbol{\tau}_N^* = J_{y,N} \nu_y \ddot{q}\hat{\mathbf{n}}_y \quad (\text{E6})$$

721 The kinematics of the rotor are:

$$722 \quad \mathbf{v}_{G,R} = \dot{q}\hat{\mathbf{t}}_x + \nu_y z_{NR} \dot{q}\hat{\mathbf{n}}_x - \nu_y x_{NR} \dot{q}\hat{\mathbf{n}}_z, \quad \boldsymbol{\omega}_R = \dot{\psi}\hat{\mathbf{e}}_{rx} + \nu_y \dot{q}\hat{\mathbf{t}}_y \quad (\text{E7})$$

$$723 \quad \mathbf{a}_{G,R} = \ddot{q}\hat{\mathbf{t}}_x + (-\nu_y^2 x_{NR} \dot{q}^2 + \nu_y z_{NR} \ddot{q})\hat{\mathbf{n}}_x + (-\nu_y^2 z_{NR} \dot{q}^2 - \nu_y x_{NR} \ddot{q})\hat{\mathbf{n}}_z \quad (\text{E8})$$

724 The corresponding Jacobians with respect to q (“1”) and ψ (“2”) are:

$$725 \quad \mathbf{J}_{v,1R} = \hat{\mathbf{t}}_x + \nu_y z_{NR} \hat{\mathbf{n}}_x - \nu_y x_{NR} \hat{\mathbf{n}}_z, \quad \mathbf{J}_{\omega,1R} = \nu_y \hat{\mathbf{t}}_y, \quad \mathbf{J}_{\omega,2R} = \hat{\mathbf{r}}_x$$

726 The inertial force and torque on the rotor are:

$$727 \quad \mathbf{f}_R^* = M_R \ddot{q}\hat{\mathbf{t}}_x + M_R (-\nu_y^2 x_{NR} \dot{q}^2 + \nu_y z_{NR} \ddot{q})\hat{\mathbf{n}}_x + M_R (-\nu_y^2 z_{NR} \dot{q}^2 - \nu_y x_{NR} \ddot{q})\hat{\mathbf{n}}_z \quad (\text{E9})$$

$$728 \quad \boldsymbol{\tau}_R^* = J_{x,R} \ddot{\psi}\hat{\mathbf{r}}_x \quad (\text{E10})$$

$$729 \quad + (J_{\oplus,R} \nu_y \sin(\psi) \dot{\psi}\dot{q} + J_{\oplus,R} (-\nu_y \sin(\psi) \dot{\psi}\dot{q} + \nu_y \cos(\psi) \ddot{q}) - J_{x,R} \nu_y \sin(\psi) \dot{\psi}\dot{q})\hat{\mathbf{r}}_y \quad (\text{E11})$$

$$730 \quad + (J_{\oplus,R} \nu_y \cos(\psi) \dot{\psi}\dot{q} + J_{\oplus,R} (-\nu_y \sin(\psi) \ddot{q} - \nu_y \cos(\psi) \dot{\psi}\dot{q}) - J_{x,R} \nu_y \cos(\psi) \dot{\psi}\dot{q})\hat{\mathbf{r}}_z \quad (\text{E12})$$

731 E2 Three-degrees-of-freedom model of a land-based or fixed-bottom wind turbine

732 The equations of motion for the model presented in subsection 4.5, with $\mathbf{q} = (q_1, q_2, \psi)$, are given in this section. The elements of the mass
733 matrix are:

$$734 \quad M_{11} = [M_{e11} + M_N + M_R] \quad (\text{E13})$$

$$735 \quad + [J_{y,N} + J_{\oplus,R} + M_N (x_{NG}^2 - 2x_{NG}q_1 + z_{NG}^2) + M_R (x_{NR}^2 - 2x_{NR}q_1 + z_{NR}^2)] \nu_y^2 \quad (\text{E14})$$

$$736 \quad + 2[M_N z_{NG} + M_R z_{NR}] \nu_y \quad (\text{E15})$$

$$737 \quad M_{13} = J_{x,R} \theta_t \nu_x \nu_y q_2 \quad (\text{E16})$$

$$738 \quad M_{22} = [M_{e22} + M_N + M_R] \quad (\text{E17})$$

$$739 \quad + [J_{x,N} + J_{x,R} + M_N z_{NG}^2 + M_R z_{NR}^2] \nu_x^2 \quad (\text{E18})$$

$$740 \quad - 2[M_N z_{NG} + M_R z_{NR}] \nu_x \quad (\text{E19})$$

$$741 \quad M_{23} = J_{x,R} \nu_x \quad (\text{E20})$$

$$742 \quad M_{33} = J_{x,R} \quad (\text{E21})$$

743 The elements of the forcing vector are:

$$744 \quad f_1 = f_{e1} - K_{e11}q_1 - D_{e11}\dot{q}_1 - J_{x,R}\theta_t\nu_x\nu_y\dot{\psi}\dot{q}_2 + [M_Nx_{NG} + M_Rx_{NR}]\nu_y^2\dot{q}_1^2 \quad (\text{E22})$$

$$745 \quad + g [M_N (\nu_y^2 z_{NG} q_1 + \nu_y x_{NG}) + M_R (\nu_y^2 z_{NR} q_1 + \nu_y x_{NR})] + f_a [\theta_t \nu_y x_{NR} - \theta_t \nu_y q_1 + \nu_y z_{NR} + 1] \quad (\text{E23})$$

$$746 \quad f_2 = f_{e2} - K_{e22}q_2 - D_{e22}\dot{q}_2 + J_{x,R}\theta_t\nu_x\nu_y\dot{\psi}\dot{q}_1 \quad (\text{E24})$$

$$747 \quad + g [M_N z_{NG} + M_R z_{NR}] \nu_x^2 q_2 + f_a \theta_t \nu_x q_2 \quad (\text{E25})$$

$$748 \quad f_3 = -J_{x,R}\theta_t\nu_x\nu_y\dot{q}_1\dot{q}_2 + \tau_a \quad (\text{E26})$$

749 E3 Three-degrees-of-freedom model of a floating wind turbine

750 The equations of motion for the model presented in subsection 4.6, with $\mathbf{q} = (x, \phi, q_T)$, are given in this section. The elements of the mass
751 matrix are:

$$752 \quad M_{11} = M_F + M_T + M_N \quad (\text{E27})$$

$$753 \quad M_{12} = M_F z_{FG} - M_{dTz} + M_N [L_T + z_{NG} - \nu_y x_{NG} q_T - \phi_y (x_{NG} + q_T + \nu_y z_{NG} q_T)] \quad (\text{E28})$$

$$754 \quad M_{13} = C_{tT1x} + M_N [1 + \nu_y z_{NG} - \nu_y^2 x_{NG} q_T - \phi_y (\nu_y^2 z_{NG} q_T + \nu_y x_{NG})] \quad (\text{E29})$$

$$755 \quad M_{22} = J_{y,F} + M_F z_{FG}^2 + J_{T,y} + J_{y,N} + M_N [(L_T^2 + z_{NG})^2 + (q_T + x_{NG})^2 + 2\nu_y q_T (z_{NG} q_T - L_T x_{NG})] \quad (\text{E30})$$

$$756 \quad M_{23} = C_{rT1y} + [J_{y,N} + M_N (x_{NG}^2 + z_{NG}^2 + L_T z_{NG} + \nu_y q_T (z_{NG} q_T - L_T x_{NG}))] \nu_y + M_N [L_T + z_{NG}] \quad (\text{E31})$$

$$757 \quad M_{33} = M_e + M_N + [J_{y,N} + M_N (x_{NG}^2 - 2x_{NG} q_T + z_{NG}^2)] \nu_y^2 + 2M_N \nu_y z_{NG} \quad (\text{E32})$$

758 The elements of the forcing vector are:

$$759 \quad f_1 = f_H + [M_F z_{FG} - M_{dz} + M_N (L_T + z_{NG} - \nu_y x_{NG} q_T)] \phi_y \dot{\phi}_y^2 + M_N [q_T + x_{NG} + \nu_y z_{NG} q_T] \dot{\phi}_y^2 \quad (\text{E33})$$

$$760 \quad + [2C_{tx} + M_N (1 + \nu_y z_{NG} - \nu_y^2 x_{NG} q_T)] \phi_y \dot{\phi}_y \dot{q}_T + M_N \nu_y [x_{NG} + \nu_y z_{NG} q_T] \dot{\phi}_y \dot{q}_T \quad (\text{E34})$$

$$761 \quad + M_N \nu_y^2 [x_{NG} + z_{NG} \phi_y] \dot{q}_T^2 \quad (\text{E35})$$

$$762 \quad + f_a [1 - \theta_t \nu_y q_T - \nu_y \phi_y q_T] \quad (\text{E36})$$

$$763 \quad f_2 = \tau_H + M_N [\nu_y^2 (L_T x_{NG} - z_{NG} q_T)] \dot{q}_T^2 \quad (\text{E37})$$

$$764 \quad - 2M_N [q_T + x_{NG} + \nu_y (2z_{NG} q_T - L_T x_{NG}) - \nu_y^2 q_T (L_T z_{NG} + x_{NG} q_T)] \dot{\phi}_y \dot{q}_T \quad (\text{E38})$$

$$765 \quad + g [M_F z_{FG} \phi_y - M_{dz} \phi_y + M_N \{(L_T + z_{NG} - \nu_y x_{NG} q_T) \phi_y + q_T + x_{NG} + \nu_y z_{NG} q_T\}] \quad (\text{E39})$$

$$766 \quad + f_a [L_T + z_{NR} + \theta_t x_{NR} + \theta_t q_T + \nu_y \dot{q}_T^2 - L_T \theta_t \nu_y q_T] \quad (\text{E40})$$

$$767 \quad f_3 = f_e - D_e \dot{q}_T - K_e q_T \quad (\text{E41})$$

$$768 \quad + M_N [q_T + x_{NG} + \nu_y (2z_{NG} q_T - L_T x_{NG}) - \nu_y^2 q_T (L_T z_{NG} + x_{NG} q_T)] \dot{\phi}_y^2 \quad (\text{E42})$$

$$769 \quad + M_N \nu_y^2 x_{NG} \dot{q}_T^2 \quad (\text{E43})$$

$$770 \quad + g [C_{tT1x} \phi_y + M_N (\nu_y x_{NG} + \nu_y^2 z_{NG} q_T - \nu_y^2 x_{NG} \phi_y q_T + \nu_y z_{NG} \phi_y + \phi_y)] \quad (\text{E44})$$

$$771 \quad + f_a [1 + \theta_t \nu_y x_{NR} - \theta_t \nu_y q_T + \nu_y z_{NR}] \quad (\text{E45})$$

772 **References**

- 773 ANSYS: <https://www.ansys.com/>, accessed: 2022-03-19, 2022.
- 774 Bauchau, O. A.: Flexible Multibody Dynamics, Solid Mechanics and Its Applications, Springer, Dordrecht, [https://doi.org/10.1007/978-94-](https://doi.org/10.1007/978-94-007-0335-3)
775 007-0335-3, 2011.
- 776 Benner, P., Gugercin, S., and Willcox, K.: A Survey of Projection-Based Model Reduction Methods for Parametric Dynamical Systems,
777 SIAM Review, 57, 483–531, <https://doi.org/10.1137/130932715>, 2015.
- 778 Bielawa, R.: Rotary wing structural dynamics and aeroelasticity, AIAA education series, American Institute of Aeronautics and Astronautics,
779 2006.
- 780 Branlard, E.: Flexible multibody dynamics using joint coordinates and the Rayleigh-Ritz approximation: The general framework behind and
781 beyond Flex, Wind Energy, 22, 877–893, <https://doi.org/10.1002/we.2327>, 2019.
- 782 Branlard, E.: WELIB, Wind Energy Library, GitHub repository <http://github.com/ebranlard/welib/>, 2021.
- 783 Branlard, E., Giardina, D., and Brown, C. S. D.: Augmented Kalman filter with a reduced mechanical model to estimate tower loads on
784 a land-based wind turbine: a step towards digital-twin simulations, Wind Energy Science, 5, 1155–1167, [https://doi.org/10.5194/wes-5-](https://doi.org/10.5194/wes-5-1155-2020)
785 1155-2020, 2020a.
- 786 Branlard, E., Jonkman, J., Dana, S., and Doubrawa, P.: A digital twin based on OpenFAST linearizations for real-time load and fatigue esti-
787 mation of land-based turbines, Journal of Physics: Conference Series, 1618, 022 030, <https://doi.org/10.1088/1742-6596/1618/2/022030>,
788 2020b.
- 789 Docquier, N., Poncelet, A., and Fiset, P.: ROBOTRAN: a powerful symbolic generator of multibody models, Mech. Sci., 4, 199–219,
790 <https://doi.org/10.5194/ms-4-199-2013>, 2013.
- 791 Gede, G., Peterson, D., Nanjangud, A., Moore, J., and Hubbard, M.: Constrained Multibody Dynamics With Python: From Symbolic Equa-
792 tion Generation to Publication., in: Proceedings of the ASME 2013 International Design Engineering Technical Conferences and Com-
793 puters and Information in Engineering Conference. Portland, Oregon, USA. August 4-7, <https://doi.org/10.1115/DETC2013-13470>, 2013.
- 794 Geisler, J.: CADynTurb: Wind Turbine Model from OpenFAST Data using CADyn Equations of Motion, [https://github.com/jgeisler0303/](https://github.com/jgeisler0303/CADynTurb)
795 CADynTurb, 2021.
- 796 G eradin, M. and Cardona, A.: Flexible Multibody Dynamics: A Finite Element Approach, Wiley, 2001.
- 797 Jeleni c, G. and Crisfield, M.: Geometrically exact 3D beam theory: implementation of a strain-invariant finite element for statics and dynam-
798 ics, Computer Methods in Applied Mechanics and Engineering, 171, 141–171, [https://doi.org/10.1016/S0045-7825\(98\)00249-7](https://doi.org/10.1016/S0045-7825(98)00249-7), 1999.
- 799 Jonkman, B., Mudafort, R. M., Platt, A., Branlard, E., Sprague, M., Jonkman, J., Vijayakumar, G., Buhl, M., Ross, H., Bortolotti, P., Masciola,
800 M., Ananthan, S., Schmidt, M. J., Rood, J., Damiani, R., Mendoza, N., Hall, M., and Corniglion, R.: OpenFAST v3.1.0. Open-source wind
801 turbine simulation tool, available at <http://github.com/OpenFAST/OpenFAST/>, <https://doi.org/10.5281/zenodo.6324288>, 2021.
- 802 Jonkman, J., Butterfield, S., Musial, W., and Scott, G.: Definition of a 5MW Reference Wind Turbine for Offshore System Development,
803 Tech. Rep. NREL/TP-500-38060, National Renewable Energy Laboratory, <https://doi.org/10.2172/947422>, 2009.
- 804 Jonkman, J. M.: Dynamics of offshore floating wind turbines—model development and verification, Wind Energy, 12, 459–492,
805 <https://doi.org/10.1002/we.347>, 2009.
- 806 Jonkman, J. M., Branlard, E., and Jasa, J. P.: Influence of wind turbine design parameters on linearized physics-based models in OpenFAST,
807 Wind Energy Science, 7, 559–571, <https://doi.org/10.5194/wes-7-559-2022>, 2022.

808 Kane, T. R. and Wang, C. F.: On the Derivation of Equations of Motion, *Journal of the Society for Industrial and Applied Mathematics*, 13,
809 487–492, <https://doi.org/10.1137/0113030>, 1965.

810 Kurtz, T., Eberhard, P., Henninger, C., and Schiehlen, W.: From Neweul to Neweul-M2: symbolical equations of motion for multibody system
811 analysis and synthesis, *Multibody System Dynamics*, 24, 25–41, <https://doi.org/10.1007/s11044-010-9187-x>, 2010.

812 Kurz, T. and Eberhard, P.: Symbolic Modeling and Analysis of Elastic Multibody Systems, in: *International Symposium on Coupled Methods*
813 in Numerical Dynamics Split, Croatia, September 16-19, 2009.

814 Lange, C., Kövecses, J., and Gonthier, Y.: Benchmarking of Multibody System Simulations: Points to Consider, in: *CcToMM Symposium*
815 on Mechanisms, Machines, and Mechatronics, Saint-Hubert, Québec, 2007.

816 Lemmer, F.: Low-order modeling, controller design and optimization of floating offshore wind turbines., Ph.D. thesis, Universit at Stuttgart,
817 <http://elib.uni-stuttgart.de/handle/11682/10543>, 2018.

818 MBDyn: <https://www.mbdyn.org/>, accessed: 2022-03-19, 2022.

819 Merz, K. O.: STAS Aeroelastic 1.0 - Theory Manual., Tech. rep., Trondheim, SINTEF Energi AS., 2018.

820 MotionGenesis: MotionGenesis™ Kane Tutorial, Tech. rep., Motion Genesis LLC, www.motiongenesis.com, 2016.

821 Øye, S.: Fix Dynamisk, aeroelastisk beregning af vindmøllevinger, Report AFM83-08, Fluid Mechanics, DTU, 1983.

822 Pöschke, F., Gauterin, E., Kühn, M., Fortmann, J., and Schulte, H.: Load mitigation and power tracking capability for wind turbines using
823 linear matrix inequality-based control design, *Wind Energy*, 23, 1792–1809, <https://doi.org/10.1002/we.2516>, 2020.

824 Reckdahl, K. and Mitiguy, P.: Autolev Tutorial, Tech. rep., OnLine Dynamics Inc., Sunnyvale CA, 1996.

825 Schwertassek, R. and Wallrapp, O.: *Dynamik flexibler Mehrkörpersysteme*. [in German], Friedr. Vieweg & Sohn, Braunschweig, 1999.

826 Shabana, A.: *Dynamics of Multibody Systems*, Dynamics of Multibody Systems, Cambridge University Press, 2013.

827 Simani, S.: Advanced Issues of Wind Turbine Modelling and Control, *Journal of Physics - Conference series*, 659, 2015.

828 Simo, J.: A finite strain beam formulation. The three-dimensional dynamic problem. Part I, *Computer Methods in Applied Mechanics and*
829 *Engineering*, 49, 55–70, [https://doi.org/10.1016/0045-7825\(85\)90050-7](https://doi.org/10.1016/0045-7825(85)90050-7), 1985.

830 SIMPACK: <https://www.3ds.com/products-services/simulia/products/simpack/>, accessed: 2022-03-19, 2022.

831 Søndersby, I. and Hansen, M. H.: Open-loop frequency response analysis of a wind turbine using a high-order linear aeroelastic model, *Wind*
832 *Energy*, 17, 1147–1167, <https://doi.org/10.1002/we.1624>, 2014.

833 Steindl, A. and Troger, H.: Methods for dimension reduction and their application in nonlinear dynamics, *International Journal of Solids and*
834 *Structures*, 38, 2131–2147, [https://doi.org/10.1016/S0020-7683\(00\)00157-8](https://doi.org/10.1016/S0020-7683(00)00157-8), 2001.

835 SymPy: <https://www.sympy.org>, 2021.

836 Touzé, C., Vizzaccaro, A., and Thomas, O.: Model order reduction methods for geometrically nonlinear structures: a review of nonlinear
837 techniques, *Nonlinear Dynamics*, 105, 1141–1190, <https://doi.org/10.1007/s11071-021-06693-9>, 2021.

838 Verlinden, O., Kouroussis, G., and Conti, C.: EasyDyn: a framework based on free symbolic and numerical tools for teaching multibody
839 systems, in: *Multibody Dynamics 2005, ECCOMAS Thematic Conference*, 2005.

840 Wallrapp, O.: Standard Input Data of Flexible Members in Multibody Systems, in: *Advanced Multibody System Dynamics. Solid Mechanics*
841 *and Its Applications*, edited by Schiehlen, W., vol. 20, pp. 445–450, Springer, Dordrecht, https://doi.org/10.1007/978-94-017-0625-4_33,
842 1993.

843 Wallrapp, O.: Standardization of flexible body modeling in multibody system codes, part i: Definition of standard input data., *Journal of*
844 *Structural Mechanics*, 22, 283–304, 1994.

845 Wallrapp, O. and Schwertassek, R.: Representation of geometric stiffening in multibody system simulation, *International Journal for Numer-*
846 *ical Methods in Engineering*, 32, 1833–1850, <https://doi.org/10.1002/nme.1620320818>, 10.1002/(ISSN)1097-0207, 1991.